UNIVERSIDADE D
COIMBRA

Rúben Filipe do Bem Gariso

MASS TRANSFER MODELS TO SUPPORT INSECTICIDE PRODUCT DEVELOPMENT

Master's dissertation in Chemical Engineering, supervised by Fernando Bernado and Mara Braga and submitted to the Department of Chemical Engineering, Faculty of Science and Technology, University of Coimbra.

October 2021

Acknowledgments/Agradecimentos

Em primeiro lugar, quero agradecer aos meus pais, Claúdia do Bem e Nuno Gariso. Obrigado por todo o apoio que me deram tanto na minha vida pessoal como no meu percurso academico. Obrigado pelo esforço económico que fizeram para que pudesse concluir o Mestrado Integrado. Obrigado por estarem sempre ao meu lado para me ouvirem mesmo quando não entendiam nada dos meus problemas no curso. Em especial ao meu pai, por ter que fazer horas extra em jardins particulares e ainda ajudar a minha mãe com as tarefas de casa, para que eu pudesse estudar. E também à mãe, por ser a minha moleta emocional. Obrigado também ao resto da família.

"Em seguida quero também agradecer ao grupo "fixes", Dani, Paula, Lopes, Sofia, Salgueiro. Obrigado por todos as gargalhadas durante os cafés nas alturas em que mais precisava. Destaco deste o Hugo e o Paredes. Obrigado por terem conseguido encontrar as palavras certas para me motivar e pela grande ajuda que me deram. E ainda para o Hugo por me ter "metido" neste grupo e por tudo o que me fez, estarei vos sempre grato.

Um obrigado também as pessoas da C.16, Joel, Eugeniu, Coutinho, Paulo e Carolina. Obrigado pela ajuda dada em pequenas dúvidas que me iam surgindo, pelas sugestões que foram dadas para melhorar a tese e por último, mas não menos importante, pelas risadas proporcionada.

Um obrigado também aos meus amigos de Soure, Camaz, Quiterio, Mariana, Jota , Henrique entre outros. Obrigado por todas os "cafés" à noite e peço desde já desculpa por ter estado ausente nestes ultimo meses, espero agora conseguir compensar a ausência. Em especial á Sofia, obrigado por apesar do que se passou, estares "sempre" disponível para me ouvir.

Agradeço a todos os professores do Departamento de Engenharia Química da FCTUC por me armarem com o conhecimento para redigir esta dissertação, em particular ao Doutor Fernando Bernardo pela grande ajuda que me deu neste grande processo da tese. Agradeço também à Doutora Mara Braga pela disponibilidade para esclarecer as duvidas em relação à parte experimental, e por último um agradecimento ao João Leocadio por ter realizado a parte experimental.

Resumo

Modelos matemáticos de transferência de massa são úteis para estudar a libertação de um ingrediente ativo (IA) e otimizar a formulação dos produtos que contêm esse IA, como acontece no caso de produtos cosméticos, farmacêuticos e inseticidas. O uso de tais modelos ajuda a compreender a relação entre a composição do produto e a velocidade de libertação do IA, e pode ainda ajudar no planeamento das experiências a realizar e assim reduzir o número de experiências necessárias. O principal objetivo da presente tese de mestrado é desenvolver modelos matemáticos que consigam prever a libertação e transporte no ar de um IA contido num produto formulado. O produto em causa está a ser desenvolvido para controlar o inseto vetor da doença da murchidão do pinheiro, usando para tal um IA que atrai o inseto para uma armadilha. A forma do produto estudada é um pequeno cilindro poroso, constituído por uma matriz polimérica sólida na qual o IA se encontra homogeneamente distribuído. O produto é fabricado usando a técnica de foaming/mixing com CO_2 supercrítico.

Foram desenvolvidos três modelos com solução analítica: um para a libertação do IA a partir do produto colocado em ar em repouso, outro para o transporte do IA num túnel de vento, e um terceiro modelo obtido pela combinação dos dois anteriores (libertação do IA seguida de transporte no túnel). Em relação ao primeiro modelo, o coeficiente de difusão efetivo do IA no interior do produto foi estimado ajustando-se o modelo a dados experimentais. Relativamente ao modelo de transporte do IA no túnel de vento, alguns dos parâmetros foram estimados usando equações conhecidas, nomeadamente os coeficientes de dispersão axial e radial do IA no túnel, em regime turbulento completamente estabelecido, e o coeficiente de partição do IA entre o produto e o ar, usando neste último caso a teoria de Flory-Huggins. Estes valores estimados serviram de ponto de partida para o ajuste ótimo do modelo a dados experimentais, minimizando-se o erro quadrático médio entre a previsão do modelo e os resultados experimentais. A solução ótima foi obtida usando o algoritmo particle swarm.

Relativamente à libertação do IA em ar em repouso, o modelo proposto descreve bem os dados experimentais, sendo nalguns casos necessário o pressuposto de que uma fração do IA não é libertada em tempo útil. Quanto ao transporte no túnel, o modelo de convecção e dispersão apresenta um erro sistemático, que é contudo de grandeza comparável à do erro experimental.

Palavras-chaves: modelação matemática da transferência de massa; solução analítica de equações de convecção dispersão; libertação de um ingrediente ativo; produtos inseticidas usando fito-

químicos.

Abstract

Mathematical models of mass transfer are useful to study the release of an active ingredient (AI) and to optimize the formulation of products that contain that AI, as is the case of cosmetics, pharmaceuticals, and insecticides. Such models may help to understand the relationship between the composition of the product and the release rate of the AI, and also may be useful in planning experiments and reducing the number of experiments needed. The main objective of this master's thesis is to develop mathematical models that can predict the release and air transport of an AI contained in a formulated product. The product in question is being developed to control the insect vector of the pine wilt disease, using an AI that attracts the insect to a trap. The shape of the studied product is a small porous cylinder, consisting of a solid polymeric matrix in which the AI is homogeneously distributed. The product is manufactured using the supercritical CO_2 foaming/mixing method.

Three models were developed with an analytical solution: one for the release of the AI from the product placed in quiescent air, a second one for the transport of the AI in a wind tunnel, and a third model obtained by combining the two previous ones (release of the AI followed by transport in the tunnel). Concerning the first model, the AI effective diffusion coefficient inside the product was estimated by fitting the model to experimental data. Regarding the AI transport model in the wind tunnel, some of the parameters were estimated using known equations, namely the longitudinal and radial dispersion coefficients of the AI in the tunnel, in a fully developed turbulent regime, and the AI partition coefficient between the product and air, using in this latter case the Flory-Huggins theory. These estimated values served as a starting point for the optimal adjustment of the model to experimental data, minimizing the mean squared error between model predictions and experimental results. The optimal solution was obtained using the particle swarm algorithm.

Regarding the release of the AI in the air at rest, the proposed model describes the experimental data well, being in some cases required the assumption that a fraction of the AI is not in fact released during the time of the release test. As for the transport in the tunnel, the convection and dispersion model has a systematic error, which is however comparable in magnitude to the experimental error.

Keywords: mass transfer mathematical modeling; analytical solution of the convection-dispersion equation; release of an active ingredient; insecticide products using phytochemicals.

Contents

List of Tables

List of Figures

Symbology

A - Transfer area (m^2)

Bi_r - Biot number in the r-direction (-)

Bi_x - Biot number in the x-direction (-)

C - Concentration of the Active Ingredient ($\mathrm{kg} \cdot \mathrm{m}^{-3}$)

C_n - Normalized concentration (-)

C_{nIC} - Normalized concentration to an infinite cylinder (-)

C_{nS} - Normalized concentration to a slab (-)

C_0 - Initial concentration of the Active Ingredient ($\mathrm{kg} \cdot \mathrm{m}^{-3}$)

C_∞ - Concentration of the Active Ingredient in the infinite ($\mathrm{kg} \cdot \mathrm{m}^{-3}$)

D - Diffusion coefficient ($\mathrm{m}^2 \cdot \mathrm{s}^{-1}$)

D_{AB} - Gas phase diffusivity of B in A ($\mathrm{cm}^2 \cdot \mathrm{s}^{-1}$)

D_M - Membrane diffusivity ($\mathrm{m}^2 \cdot \mathrm{s}^{-1}$)

D_r - Radial dispersion coefficient ($\mathrm{m}^2 \cdot \mathrm{s}^{-1}$)

D_z - Longitudinal dispersion coefficient ($\mathrm{m}^2 \cdot \mathrm{s}^{-1}$)

H - Height of the monolith (m)

K^{eff} - Partition coefficient of the porous monolith (-)

k_{m_r} - Mass transfer coefficient for the AI from in air for the r-direction ($\mathrm{m} \cdot \mathrm{s}^{-1}$)

k_{m_x} - Mass transfer coefficient for the AI from in air for the x-direction ($\mathrm{m} \cdot \mathrm{s}^{-1}$)

K^{teo} - Partition coefficient to the non-porous monolith (-)

K_1 - Partition coefficient between the monolith and the membrane (-)

K_2 - Partition coefficient between the membrane and the air (-)

L_M - Membrane thickness (m)

M - Amount released from time 0 to time t (kg)

M_i - Molar mass of the compound i ($\mathrm{g} \cdot \mathrm{mol}^{-1}$)

M_∞ - Amount released from time 0 to time ∞ (kg)

P - Pressure (atm)

P_{mem} - Membrane permeability ($\mathrm{m} \cdot \mathrm{s}^{-1}$)

Q - Amount released ($\mathrm{kg} \cdot \mathrm{s}^{-1}$)

R - Radius (m)

Re - Reynolds number (-)

R_1 - Cylinder radius (m)

R_2 - Tunnel radius (m)

T - Temperature (K)

u - Wind velocity ($\mathrm{m} \cdot \mathrm{s}^{-1}$)

w_i - Weight fraction of component i (-)

α - Scaled longitudinal dispersion coefficient (-)

α_r - Fraction of active ingredient that can be released easily (-)

β - Scaled radial dispersion coefficient (-)

δ - Ratio of the radius of the tunnel where the injection occurs (-)

ϵ - Porosity (-)

ρ - density of the fluid ($\mathrm{kg} \cdot \mathrm{m}^{-3}$)

ϕ_1 - Normalized concentration modified in a stationary-state (-)

χ - Flory interaction parameter (-)

Abbreviation

1D - One-dimension

2D - Two-dimension

3D - Three-dimension

AI - Active Ingredient

CDE - Convection-dispersion equation

ODE - Ordinary differential equation

PDE - Partial differential equation

PCL - Poly(ϵ-carprolactone)

PSO - Particle Swarm Optimization

PWD - Pine wilt disease

PWN - Pinewood nematode

RMSE - Root Mean Squared Error

Chapter 1

Introduction

The release of an active ingredient (AI) is a pivotal function in a wide range of products, including pharmaceuticals, foods, personal care products, home fragrance products, and insecticides (Chen *et al.*, 2019; Lian *et al.*, 2004; Siepmann and Siepmann, 2012; Vergnaud, 1993) . In the present thesis, the solid-gas release of an insecticide is modeled mathematically. This work has been conducted inside a larger project called *Ecovector*.

The *Ecovector* project (Braga, 2020) aims to control pine wilt disease (PWD). *Pinus* is the main host for the pinewood nematode (PWN) (*Bursaphelenchus xylophilus*), which is the causal agent for PWD, and transmission from one tree to another requires an insect vector. In Portugal, the only vector present is the *Monochamus galloprovincialis*. The principal objective is to develop a formulated product to control the transmission of PWN using volatile phytochemicals as AIs that attract insects to a trap (or in some cases AIs that have a repellent effect). Other materials are used to formulate the product and those should be biodegradable (polymeric supports, coating, and eventually other auxiliary ingredients) (Braga, 2020). This product needs to have a prolonged effect (several days or even weeks) and be active up to a certain distance (1 meter or more). Activity here means that the product provides an AI concentration in the surrounding air sufficiently high to attract insects.

In order to study the release rate of the AI, two main experimental trials were done: release of the AI from the product under quiescent air, and a second experience (named wind tunnel) where the product is placed in a tunnel and air is forced to pass through it dragging the released AI. The concentration of the AI in the gas phase is measured along the tunnel (Braga, 2020; Bernardo *et al.*, 2019).

Notably, modeling the release of the AI as a mass transfer process is a valuable tool to formulate the product, since its composition affects the release profile. A model could be used to predict the experimental result, helping to reduce the number of experiences needed and also to plan the most informative ones. A reliable model could, in theory, be used to determine what product composition and what production process conditions are required to attain a specific

performance.

The principal goal of the present thesis is to create models that can reliably describe the experiences made in the *Ecovector* project. Those models need to be validated, first adjusting the main model parameters to a set of tests, and then using the models in a predictive way, comparing predictions without parameters adjustment with a different set of experimental data.

To achieve the principal goal, two phenomena were studied, and in both cases using analytical solutions of the transport equations: AI diffusion out of the product and transport in the tunnel (convection and dispersion). The wind tunnel experience was modeled using a new approach that combines the two analytical solutions, being thus proposed an overall analytical model able to describe the release of the AI followed by the transport in the tunnel.

The thesis is divided into 8 chapters.

Chapter 2 reviews the existent solution to diffusion and convection + dispersion problems, and also, model fitting solutions approaches based on optimization.

Chapter 3 summarizes the experimental part done in the *Ecovector* project, not done in this work, but necessarily important to construct suitable models.

Chapter 4 presents the developed models and their analytical solutions.

Chapter 5 presents the equations used to estimate some of the model parameters (e.g., partition and dispersion coefficients).

Chapter 6 exhibits the computational strategy adopted.

Chapter 7 shows the results of both model fitting and model prediction, and also discusses some model limitations.

Last but not least, Chapter 8 presents the conclusions of this thesis and also possible future work.

Chapter 2

State of art

2.1 Modeling transport phenomena

In this chapter, the modeling of two different phenomena will be reviewed: the release of an active ingredient (AI) from a solid product by diffusion, and convection-dispersion of an AI in cylindrical geometry.

2.1.1 Active ingredient diffusion out of a solid product

Different types of mass transport processes can be involved in the release of an AI from a solid product containing it. Often, diffusion is the rate-controlling phenomenon. To quantify it, Equation 2.1 (Siepmann and Siepmann, 2012)) can be applied, if the product geometry is defined in Cartesian coordinates. The initial and boundary conditions differ from case to case and thus the solution of Equation 2.1 will also change.

$$\frac{\partial C}{\partial t} = D\left(\frac{\partial^2 C}{\partial x^2} + \frac{\partial^2 C}{\partial y^2} + \frac{\partial^2 C}{\partial z^2}\right) \tag{2.1}$$

where:

$C(x, y, z, t)$ is the AI concentration in the product;

D is the diffusion coefficient;

t is the time;

x, z and y are the Cartesian coordinates.

2.1.2 Active ingredient convection-dispersion in cylindrical geometry

The convection-dispersion equation (CDE) has been widely used to describe the transport of a tracer or a solute in a given flow system. The CDE can be used in a variety of areas such as in hydrological (Chen *et al.*, 2011b) and environmental (Chen *et al.*, 2011a) sciences. The CDE

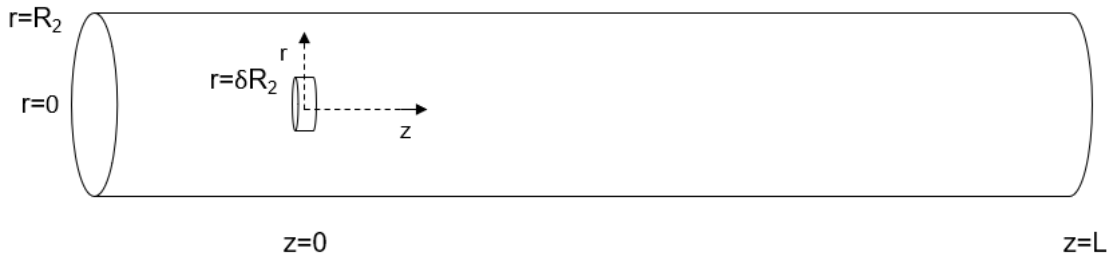

Figure 2.1: Sketch of the flow system in cylindrical coordinates.

can be in one (1D), two (2D), or three (3D) dimensions, and is subject to various initial and boundary conditions. The CDE in cylindrical coordinates (Figure 2.1), and in a fluid flowing in the longitudinal direction with mean velocity u, is given by Equation 2.2.

$$\frac{\partial C}{\partial t} + u\frac{\partial C}{\partial z} = D_z\frac{\partial^2 C}{\partial z^2} + D_r\left(\frac{\partial^2 C}{\partial r^2} + \frac{1}{r}\frac{\partial C}{\partial r}\right) \tag{2.2}$$

for:

$$0 < z < L \tag{2.3a}$$

$$0 < r < R_2 \tag{2.3b}$$

$$t > 0. \tag{2.3c}$$

Here:

z and r are the longitudinal and the radial coordinate;

L and R_2 are the length and radius of the tunnel;

$C(z, r, t)$ represents the solute concentration;

u is the fluid velocity in the tunnel;

D_z and D_r is the longitudinal and radial dispersion coefficients, respectively;

Usually, the initial condition is:

$$C\,(z, r, 0) = 0. \tag{2.4}$$

The inlet boundary condition (for $z = 0$) differs from case to case, but the commonly used are the first-type condition (concentration equals to a known C_0 [Equation 2.5]) or the third-type condition (transfer rate per unit are equals to a known value q_0 [Equation 2.6]) (Leij *et al.*, 1991). When these conditions only apply to a subdomain of r, one has the following equations:

$$C\,(0, r, t) = \begin{cases} C_0, & 0 \le r \le \delta R_2. \\ 0, & \delta R_2 < r \le R_2. \end{cases} \tag{2.5}$$

$$u\,C\,(0,r,t) - D_z\frac{\partial C}{\partial z} = \begin{cases} u\,q_0 & 0 \leq r \leq \delta R_2. \\ 0, & \delta R_2 < r \leq R_2. \end{cases} \tag{2.6}$$

Usually, the others boundary conditions are:

$$\left.\frac{\partial C}{\partial z}\right|_{z=L} = 0 \tag{2.7a}$$

$$\left.\frac{\partial C}{\partial r}\right|_{r=0} = 0 \tag{2.7b}$$

$$\left.\frac{\partial C}{\partial z}\right|_{r=R_2} = 0. \tag{2.7c}$$

2.2 Analytical *versus* numerical solution

Only very few Partial Differential Equations (PDEs) have the analytical or exact solution. Most of the time, anyone who wants to develop and use models based on such equations and their associated conditions must be able to obtain numerical solutions efficiently and accurately (Hutomo *et al.*, 2019).

To obtain an analytical solution, the PDE should be linear (relatively to independent variables, dependent variable, and all derivatives), and have constant parameters (i.e., diffusion/dispersion coefficients) (Hutomo *et al.*, 2019; Siepmann and Siepmann, 2012). If these criteria are not met, even in the case of only one non-linear term or only one non-constant parameter (Hutomo *et al.*, 2019; Siepmann and Siepmann, 2012).

2.2.1 Analytical solution

Diffusion equation

The release of an AI from polymeric support can be modeled according to how the AI is dissolved in that support.

Siepmann and Siepmann (2012) review the analytical solution for the cases where the AI is homogeneously dispersed throughout the support (called monolith), and for the case where the AI and the support are "completely" physically separated (the AI is located at the center of the product, whereas the polymer forms a membrane surrounding the reservoir of AI). The solutions present are only for the infinite slab, sphere, and cylinder geometries. Also, Vergnaud (1993) compiled several solutions for a wide range of boundary and initial conditions, including for the case where the external resistance is not negligible when compared with the internal one.

Convection-dispersion equation

Several analytical solutions for the CDE in Cartesian coordinates have been derived in the literature. For instance, Van Genuchten (1982) compiled several analytical solutions to the 1D CDEs with various initial and boundary conditions. Batu (1989, 1993) presents analytical solutions for the 2D CDE. Batu (1996),Leij *et al.* (1991), and Park and Zhan (2001) derived 3D solutions.

Leij *et al.* (1991) derived an analytical solution for 2D CDE in cylindrical coordinates subject to first-type (Equation 2.5) and third-type (Equation 2.6) inlet conditions using Laplace and Hankel transform techniques. Hwang (2021) also develop an exact solution to the previous case using the Fokas method (also known as unified transformations).

The method of separation of variables combined with the principle of superposition is widely used to solve initial and boundary conditions problems. Usually, the dependent variable (u) is expressed in the separable form $u(x, y) = X(x)Y(y)$, where X and Y are functions of only x and only y, respectively. In many cases, the PDE reduces to two ordinary differential equations (ODEs) for X and Y (Myint-U and Debnath, 2007).

However, the question of the separability of a partial differential equation into two or more ODEs is by no means an easy one. Despite this, the method of separation of variables is extensively used in finding solutions to a large class of initial and boundary conditions problems (Myint-U and Debnath, 2007).

2.2.2 Numerical solution

The oldest and most method used for obtaining the numerical solution of a PDE is the finite difference method (Finlayson, 1980). Also, there are methods based on finite elements (Finlayson, 1980) or boundary elements (Katsikadelis, 2002).

There are numerous numerical solutions to 2D or 3D CDE with the uniform flow and constant coefficients (for example Dehghan (2007), Thongmoon and McKibbin (2006), and Thongmoon *et al.* (2012)). In Hutomo *et al.* (2019) the 2D CDE was developed with variable coefficients by using the Du-Fort Frankel method (a development of the finite difference method).

2.3 Model fitting

If one or several of the parameters needed for obtaining the solution are unknown, the model equations can be "fitted" to sets of experimental data. This means that the unknown parameters are optimized to minimize the differences between experimental and theoretical data points. This could be achieved using the criterion of Root Mean Squared Error (RMSE) (Equation 2.8).

$$RMSE = \sqrt{\frac{\sum_{i=1}^{N}(y_{expi} - y_{modi})^2}{N}} \tag{2.8}$$

here:

y_{expi} is the experimental value;

y_{modi} is the value predicted by the model;

N is the number of experimental points.

To find the optimum of a given function, several approaches are possible. Despite a wide range of optimization algorithms, there is not a method that could be considered the best for any case. To solve this problem, one must understand different optimization methods. In general, optimization methods are divided into heuristic and derivative-based methods (Edgar *et al.*, 2001).

There are also a growing number of publications regarding a hybrid formulation of optimization algorithms, using a combination of heuristic and derivative-based methods (Dominković *et al.*, 2015; Nery and Rolnik, 2007b; Zadeh *et al.*, 2015).

2.3.1 Derivative-based method

Derivative-based methods aim to establish an iterative optimization algorithm that uses information on the first derivative (and sometimes also of the second derivative) of the objective function. Three examples of derivative-based methods are: conjugated gradient, Newton, and Quasi-Newton methods (Edgar *et al.*, 2001).

2.3.2 Heuristic methods

Unlike the previous methods, heuristic methods does not use information about the objective function gradient and are not very sensitive to initial parameter guesses. Further, they can be more easily used for global optimization, through extensive calculation of the objective function in the space of the optimization variables (Edgar *et al.*, 2001).

Many works have already reported the uses of heuristic methods to perform parameter model estimation and data reconciliation such as Genetic Algorithm ((Marseguerra *et al.*, 2003; Park and Froment, 1998; Schwaab and Chalbaud, 2008)), Simulated Annealing ((Eftaxias *et al.*, 2002)), and Particle Swarm Optimization (PSO) (Kennedy and Eberhart, 1995).

Sarkar *et al.* (2013) show that PSO allows for improved parameter estimation with less computational effort when compared with the others.

Particle Swarm Optimization

The PSO technique was originally proposed by Kennedy and Eberhart (1995), based on the social behavior of a collection of animals. Each individual of the swarm, called a particle, remembers the best solution found by itself and by the whole swarm along the search trajectory. Particles move along the search space and exchange information with other particles.

2.3.3 Hybrid Method

Hybrid methods represent a combination of derivative-based and heuristic methods to exploit the advantage of both classes of methods.

Typically, hybrid methods first use a heuristic method to locate the region where the global minimum likely is. Once this region is determined, the hybrid formulation algorithm switches to a derivative-based method to get closer and faster to the minimum point (Almeida and Coppo Leite, 2019; Edgar *et al.*, 2001).

Dominković *et al.* (2015), Mohammad Zadeh *et al.* (2015), and Nery and Rolnik (2007a) showed the efficiency and effectiveness of hybrid models.

Chapter 3

Experimental methods

This chapter summarizes the experimental part performed inside the *Ecovector* project, not done in this work, but necessarily important to construct suitable models.

3.1 Product form

The basic product form studied is a small porous cylinder, composed of a polymer and the active ingredient (AI). This one is homogeneously dispersed in the polymeric matrix and for that reason, this product form is called a monolith. Two variants of this product form were studied: (i) only the monolith; (ii) the monolith covered with a membrane.

(a) Front view **(b)** Top view

Figure 3.1: Example of an experimentally obtained monolith.

The *Ecovector* project aims to use natural products to attract or repel the insect vector. In nature, α-pinene is known to attract the vector and eucalyptol to repel it. These compounds were chosen as AIs. Mixtures of AIs are also under study, but that case is not here reported (de Matos *et al.*, 2015; Goimil *et al.*, 2017). Currently, only were used pure AI. However, a mixture of different AIs is being studied. For the present thesis poly(ϵ-caprolactone) (PCL) was chosen as the polymeric support. The membrane is regenerated cellulose and has a thickness of $0.1\mathrm{mm}$.

The monoliths (present in Figure 3.1) are manufactured by supercritical carbon dioxide (CO_2) foaming/mixing method. Pure PCL powder is mixed with liquid AI and the mixture is introduced into cylinder molds and then processed by supercritical carbon dioxide foaming/mixing method under different temperature and pressure conditions, corresponding to different supercritical CO_2 densities (see Table 3.1) (de Matos *et al.*, 2015; Goimil *et al.*, 2017).

Table 3.1: List of experiments (Bernardo *et al.*, 2019).

Experiment	AI	Temperature ($^{\circ}C$)	Pressure (bar)	membrane
Exp1	α-pinene	45	189	no
Exp2	α-pinene	35	139	no
Exp3	α-pinene	40	133	no
Exp4	α-pinene	40	164	no
Exp5	α-pinene	40	212	no
Exp6	α-pinene	40	133	yes
Exp7	eucalyptol	40	133	no
Exp8	eucalyptol	40	164	no
Exp9	eucalyptol	40	212	no
Exp10	eucalyptol	40	133	yes

AI release tests are made at least in duplicate and for each experiment, a new monolith needs to be produced. This leads to some disparity in the cylinder dimensions (radius (R), height (H), porosity (ϵ), and initial AI concentrations (C_0)). Table 3.2 shows the average values of these parameters (in the cases of C_0, mean value ± standard deviation).

Table 3.2: Monolith dimensions, porosity, and initial AI concentration for several experiments (Bernardo *et al.*, 2019).

	AI release		wind tunnel			
Experiment	R (cm)	H (cm)	R (cm)	H (cm)	ϵ (-)	C_0 ($\mathrm{kg \cdot m^{-3}}$)
Exp1	-	-	0.81	3.20	0.841	127±8
Exp2	-	-	0.81	2.20	0.797	175±9
Exp3	0.80	2.20	0.80	2.25	0.776	194±14
Exp4	0.80	2.00	0.80	2.20	0.762	190±28
Exp5	0.80	2.30	0.80	2.10	0.792	173±12
Exp6	0.80	2.25	-	-	-	-
Exp7	0.75	2.50	0.75	2.75	0.788	176±5
Exp8	0.75	2.40	0.75	2.55	0.789	187±12
Exp9	0.75	2.65	0.75	2.50	0.801	149±47
Exp10	0.75	2.60	-	-	-	-

3.2 Active ingredient passive release

The monolith is placed on a scale, as shown in Figure 3.2, and under quiescent air conditions, the mass lost is measured by gravimetric assays. This test is also used to determine the initial load (C_0) and the porosity (ϵ).

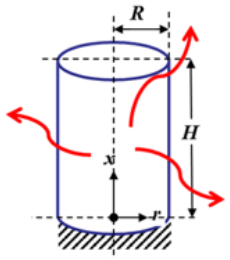

Figure 3.2: Sketch of active ingredient release from a cylinder.

For example, for experience Exp3-replica1, the mass loss over time is present in Figure 3.3, with the y axis being:

$$\frac{M}{M_\infty} = \frac{Y_{initial} - Y_i}{Y_{initial} - Y_{last}}$$

where:

$Y_{initial}$ is the mass of the monolith at the beginning of the experience;

Y_i is the mass in a given time;

Y_{last} is the last mass measure.

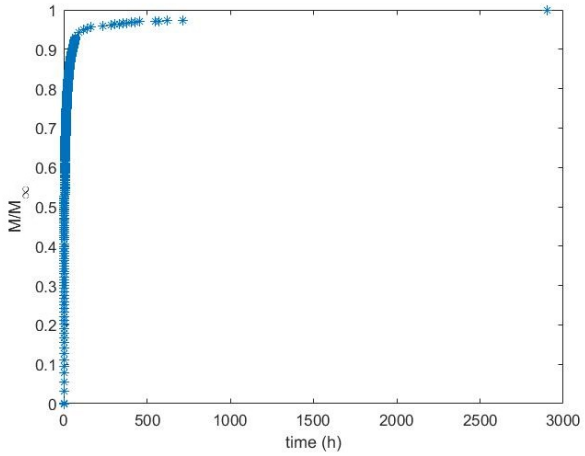

Figure 3.3: Experimental data for Exp3 (Bernardo *et al.*, 2019).

As Figure 3.3 shows, in the first couple of hours (approximately 70 h), the release rate is must faster than the rest. Only the first 70 h were used in the parameter fitting and are present in Figure 3.3.

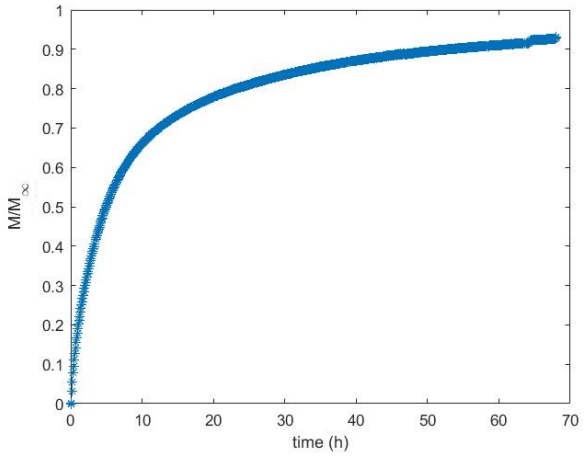

Figure 3.4: Experimental data to Exp3, zoom for the first 70 h (Bernardo *et al.*, 2019).

Given that the mass lost is measured by gravimetry, this experience can only give information about the total mix of the AIs as one and can not differentiate between them. Contrary to this, the experience below (explained 3.3), can differentiate between AIs.

3.3 Active ingredient release and dispersion in a wind tunnel

Figure 3.5 shows a sketch of the cylindrical wind tunnel. The product (monolith) is placed on the tunnel axis, 1 meter away from the entrance, where the air fan is located. The concentration of AI is measured through adsorption fibers that are first exposed to the flowing air until saturation (a few seconds) and then analyzed by SPME-GC-MS (Bernardo *et al.*, 2019) (that can detect different species).

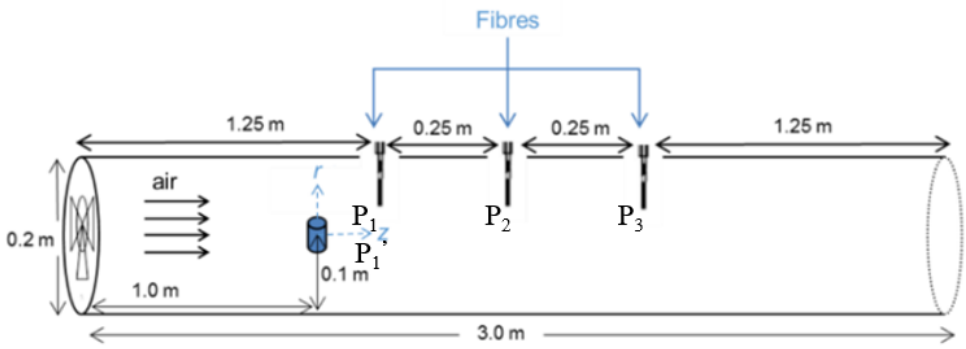

Figure 3.5: Schematic representation of the wind tunnel.

The four selected positions, in cylindrical coordinates (z,r), are: P_1(0.25,0.035), $P_1^{'}$(0.25,0.085), P_2(0.50,0.035) and P_3(0.75,0.035) (values in m; the product is placed at the origin (0,0), as seen in Figure 3.5). The concentration in these four points is measured at different times after the beginning of the assay. Different experiences used different positions, and that information can be consulted in Table 3.3.

For example, to experience Exp1, experimental data to the fours point are present in Figure 3.6.

Table 3.3: Experimental tunnel points.

Experiment	$P_1^{'}$	P_1	P_2	P_3
Exp1	yes	yes	yes	yes
Exp2	yes	yes	yes	yes
Exp3	no	no	no	yes
Exp4	no	no	no	yes
Exp5	no	no	no	yes
Exp6	no	no	no	yes
Exp7	no	no	yes	yes
Exp8	no	no	yes	yes
Exp9	no	no	yes	yes

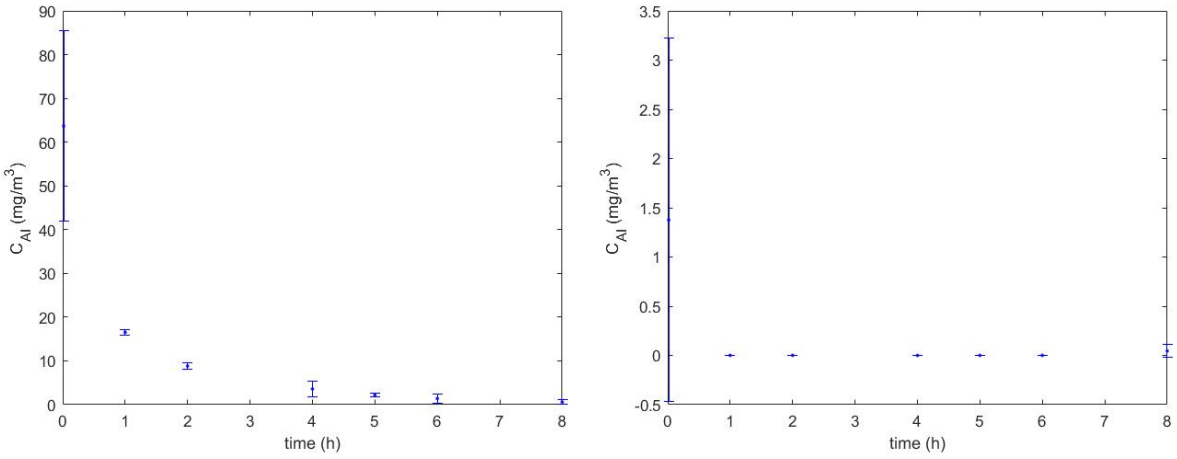

(a) Point P_1

(b) Point $P_1^{'}$

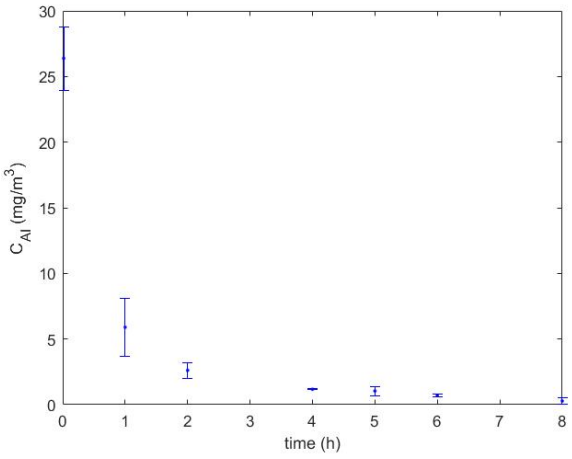

(c) Point P_2

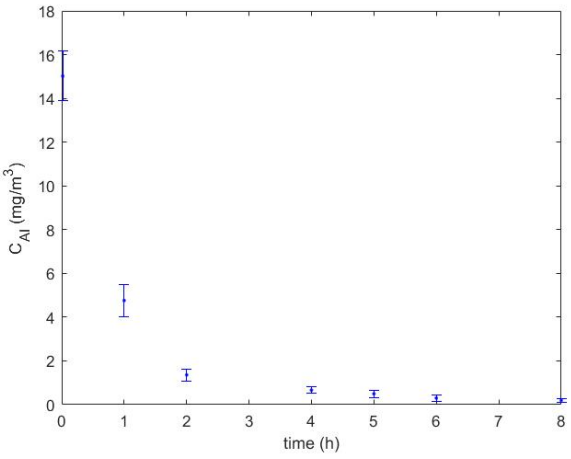

(d) Point P_3

Figure 3.6: Experimental data for Exp1 at different points in the tunnel (Bernardo *et al.*, 2019).

Wind velocity (u) is measured using an anemometer placed 0.5 m or 0.75 m from the position of the monolith at the center of the tunnel. The velocity wasn't experimentally measured in the present thesis. However, this parameter was measured in experiments performed afterward.

The mean velocity of those experiences is $u = 0.685\ \mathrm{m} \cdot \mathrm{s}^{-1}$. This value is considered the value of all experiences.

Chapter 4

Models

4.1 Model description

In this chapter are developed models for three different cases:

- Active ingredient (AI) release from a monolith, under quiescent condition (model I);
- AI dispersion in a wind tunnel in a stationary state (model II);
- AI release from a monolith followed by dispersion in a wind tunnel (model I + II).

The monolith is modeled, as a finite cylinder (Figure 3.2), without having into consideration the microstructure (this means a pseudo-homogeneous mixture).

The release has the following mass transport mechanisms in series (presented in Figure 4.1):

- diffusion inside the cylinder;
- diffusion into the membrane;
- diffusion into the air.

Firstly, a model with the three mechanisms (or transfer-resistant) was built (Section 4.3.1) and then simplified. Three simplified models were all made:

- without membrane resistance (Section 4.3.2);
- without membrane and air resistances (Section 4.3.3);
- without air resistance (Section 4.3.4).

As explained in Chapter 3, the release is faster in the initial hours. Then, a modification of the previous model is built where only a fraction of the AI is released (Section 4.3.5).

For model II, all the AI is introduced in the center of the tunnel at a point where there are no entrance effects, and the profile is fully developed (present in Figure 3.5).

The third model (model I + II) is the combination of the previous two models, the monolith

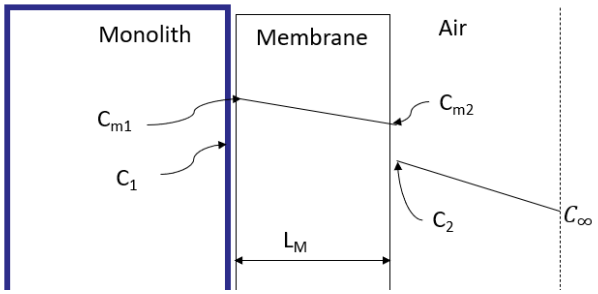

Figure 4.1: Active ingredient concentrations in the monolith, membrane, and air.

is placed at the center of the tunnel and approximated to a flat disc of which radius is a small fraction of the tunnel radius (δ).

4.2 Analytical solution

Models with the analytical solution were chosen, due to having some advantages, such as the accuracy is high and can be easily controlled when infinite series are present (develop in the following sections), also, the equations are linear meaning that, parameters such as the membrane diffusivity, diffusion coefficient, coefficient of dispersion in the tunnel, and the velocity of the air are constant values.

Since those equations are linear, the optimization process is much effortless given that the solution does not need past information to get the value for a given time and spatial point and thus, has less computational effort.

When infinite series are present, it is possible to determine the exact number of digits correct in the approximation of the series.

A method to find the roots used in the infinite series should have good accuracy to not miss any root, but if the time needed is too high, this may become a disadvantage when compared with the numerical solution. So, the method used needs to be accurate but at the same time quick.

4.3 Model I: Active ingredient release from a monolith

4.3.1 Monolith with membrane and transfer to air

he mass balance to the AI inside the cylindrical product and corresponding initial condition and four boundary conditions are (see Figure 4.2):

$$\frac{\partial C}{\partial t} = D\frac{\partial^2 C}{\partial x^2} + D\left(\frac{\partial^2 C}{\partial r^2} + \frac{1}{r}\frac{\partial C}{\partial r}\right) \tag{4.1a}$$

$$C\,(0, x, r) = C_0 \tag{4.1b}$$

$$\left.\frac{\partial C}{\partial r}\right|_{r=0} = 0 \tag{4.1c}$$

$$\left.\frac{\partial C}{\partial x}\right|_{x=0} = 0 \tag{4.1d}$$

$$-D\left.\frac{\partial C}{\partial x}\right|_{x=H} = k_x(K_1 C(t, H, r) - K_2 C_\infty) \tag{4.1e}$$

$$-D\left.\frac{\partial C}{\partial r}\right|_{r=R_1} = k_r(K_1 C(t, x, R_1) - K_2 C_\infty) \tag{4.1f}$$

where:

C is the concentration of AI in the monolith ($kg_{IA}\ m^{-3}_{monolith}$) and the others C are portrayed in Figure 4.1;

D is effective diffusion coefficient ($\mathrm{m}^2 \cdot \mathrm{s}^{-1}$);

k_x is the global transfer mass coefficient for the AI from monolith to air for the x-direction with unites of concentration of the AI in the membrane ($\mathrm{m} \cdot \mathrm{s}^{-1}$);

k_r is the global transfer mass coefficient for the AI from monolith to air for the r-direction with unites of concentration of the AI in the membrane ($\mathrm{m} \cdot \mathrm{s}^{-1}$);

K_1 is the partition coefficient between the monolith and the membrane (-) (Equation 4.2a);

K_2 is the partition coefficient between the membrane and the air (-) (Equation 4.2b).

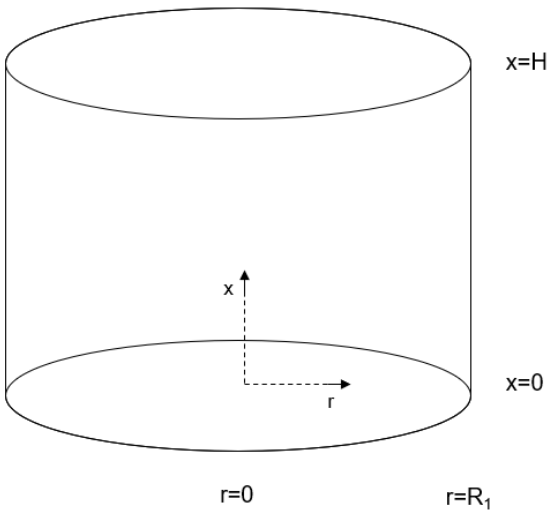

Figure 4.2: Sketch of the monolith.

$$K_1 = \frac{C_{m1}}{C_1} \tag{4.2a}$$

$$K_2 = \frac{C_{m2}}{C_2}. \tag{4.2b}$$

The values of k_r and k_x will be now deducted.

In the x-direction, the transfer rate, considering a linear profile, through the membrane (J_x) is:

$$J_x = \frac{D_M A_x}{L_M} \left(C_{m1} - C_{m2}\right) \tag{4.3}$$

where:

A_x is the transfer area (m^2);

D_M is membrane diffusivity ($\mathrm{m}^2 \cdot \mathrm{s}^{-1}$);

L_M is membrane thickness (m).

In the air, the transfer rate, considering a linear profile (J_x) is:

$$J_x = k_{m_x} A_x \left(C_2 - C_\infty\right) \tag{4.4}$$

where k_{m_x} is the mass transfer coefficient for the AI from in the air for the x-direction ($\mathrm{m} \cdot \mathrm{s}^{-1}$).

Considering the definitions of K_1 and K_2, and that the transfer rate in the air and through the membrane are equal (Çengel and Ghajar, 2015):

$$J_x = k_x A_x \left(K_1 C\left(t, H, r\right) - K_2 C\infty\right) \ . \tag{4.5}$$

For the r-direction, the same conclusion can be reached (Çengel and Ghajar, 2015):

$$J_r = k_r A_r \left(\alpha_1 C\left(t, x, R_1\right) - \alpha_2 C_\infty\right) \tag{4.6}$$

with:

$$k_x = \frac{1}{\frac{L_M}{D_M} + \frac{K_2}{k_{m_x}}} \tag{4.7a}$$

$$k_r = \frac{1}{\frac{L_M}{D_M} + \frac{K_2}{k_{m_r}}} \tag{4.7b}$$

$$A_x = \pi R_1^2 \tag{4.7c}$$

$$A_x = 4\pi R_1 H \tag{4.7d}$$

where k_{m_r} is the mass transfer coefficient for the AI from in the air for the r direction ($\mathrm{m} \cdot \mathrm{s}^{-1}$).

The analytical solution is obtained as the product of two one-dimensional solutions: (slab of thickness 2H) × (infinite cylinder of radius R_1):

$$C_n = \frac{K_1 C\left(t, x, r\right) - K_2 C_\infty}{K_1 C_0 - K_2 C_\infty} = C_{nS} C_{nIC}. \tag{4.8}$$

Where (Incropera *et al.*, 2017):

$$C_{nIC}\left(t_{nr}, r_n, Bi_r\right) = \sum_{i=1}^{\infty} a_{ri} \exp(-b_{ri}^2 t_{nr}) J_0(b_{ri} r_n) \tag{4.9a}$$

$$C_{nS}\left(t_{nx}, x_n, Bi_x\right) = \sum_{i=1}^{\infty} a_{xi} \exp(-b_{xi}^2 t_{nx}) \cos(b_{xi} x_n) \tag{4.9b}$$

with:

$$a_{ri} = \frac{2Bi_r}{\left(b_{ri}^2 + Bi_r^2\right) J_0(b_{ri})} \tag{4.10a}$$

$$a_{xi} = \frac{2Bi_x}{\left(b_{xi}^2 + Bi_x^2 + Bi_x\right) \cos\left(b_{xi}\right)} \,. \tag{4.10b}$$

Where b_{xi} and b_{ri} are the roots of Equations 4.11a, 4.11b, respectively (Incropera *et al.*, 2017):

$$b_{xi} \sin b_{xi} = Bi_x \cos b_{xi} \tag{4.11a}$$

$$b_{ri} J_1\left(b_{ri}\right) = Bi_r J_0\left(b_{ri}\right). \tag{4.11b}$$

where J_0 and J_1 are the Bessel function of order 0 and 1, respectively, of the first kind.

With the following normalized variables:

$$t_{nx} = \frac{Dt}{H^2} \tag{4.12a}$$

$$t_{nr} = \frac{Dt}{R_1^2} \tag{4.12b}$$

$$x_n = \frac{x}{H} \tag{4.12c}$$

$$r_n = \frac{r}{R_1}. \tag{4.12d}$$

The normalized boundary conditions are now:

$$\left.\frac{\partial C_n}{\partial r_n}\right|_{r_n=0} = 0 \tag{4.13a}$$

$$\left.\frac{\partial C_n}{\partial x_n}\right|_{x_n=0} = 0 \tag{4.13b}$$

$$\left.\frac{\partial C_n}{\partial r_n}\right|_{r_n=1} = -\mathrm{Bi}_r C_n\left(t_n, x_n, 1\right) \tag{4.13c}$$

$$\left.\frac{\partial C_n}{\partial x_n}\right|_{x_n=1} = -Bi_x C_n\left(t_n, 1, r_n\right). \tag{4.13d}$$

With Biot number in the x-direction (Bi_x) and Biot number in the r-direction (Bi_r):

$$Bi_x = \frac{k_x H K_1}{D} \tag{4.14a}$$

$$Bi_r = \frac{k_r R_1 K_1}{D} \tag{4.14b}$$

The amount released ($Q(\mathrm{kg}\cdot\mathrm{s}^{-1})$) is equal to the sum of AI that disperses either in a radial or axial direction $Q(t) = Q_x + Q_r$.

$$Q = 2\int_0^{R_1} D_x 2\pi r \left.\frac{\partial C}{\partial x}\right|_{x=H} dr + 2\int_0^{H} D_r 2\pi R_1 \left.\frac{\partial C}{\partial r}\right|_{r=R_1} dx. \tag{4.15}$$

Combining Equations 4.13d, 4.13c and 4.8 one obtains:

$$\left.\frac{\partial C_n}{\partial x_n}\right|_{x_n=1} = -Bi_x C_{nS}(t_n, 1) C_{nIC}(t_n, r_n) \tag{4.16a}$$

$$\left.\frac{\partial C_n}{\partial r_n}\right|_{r_n=1} = -Bi_x C_{nS}(t_n, x_n) C_{nIC}(t_n,). \tag{4.16b}$$

Solving Equation 4.15 with Equations 4.16b 4.16a:

$$Q\left(t_n\right) = \left(k_r f_r A_r K_1 \; + k_x f_r A_x K_1\right)\left(K_1 C_0 - K_2 C_\infty\right) \tag{4.17}$$

where:

$$f_x = 2C_{nS}(t_n, 1) \int_0^1 C_{nIC}\,(t_n, r_n)\, r_n dr_n \tag{4.18a}$$

$$f_r = C_{nIC}(t_n, 1) \int_0^1 C_{nS}\,(t_n, x_n)\, dx_n \tag{4.18b}$$

with:

$$\int_0^1 C_{nIC}\,(t_n, r_n)\, r_n dr_n = \sum_{i=1}^{\infty} \frac{a_{ri} \exp(-b_{ri}^2 t_{nr}) J_1(b_{ri})}{b_{ri}} \tag{4.19a}$$

$$\int_0^1 C_{nS}\,(t_n, x_n)\, dx_n = \sum_{i=1}^{\infty} \frac{a_{xi} \exp(-b_{xi}^2 t_{nx}) \sin(b_{xi})}{b_{xi}}. \tag{4.19b}$$

With:

a_{xi} and a_{ri} are defined in Equations 4.10b and 4.10a;

b_{xi} and b_{ri} are the roots of Equations 4.11b and 4.11a.

The amount released (M) from time 0 to time t is given by:

$$M = \int_0^t Q\,(t)\, dt. \tag{4.20}$$

For a slab is possible to find an analytic equation for the ratio between the mass for a given t and the total mass (Vergnaud, 1993):

$$\left(\frac{M}{M_\infty}\right)_S = 1 - \sum_{i=1}^{\infty} \frac{2Bi_x^2 \exp\left(-b_{xi}^2 t_{nx}\right)}{b_{xi}^2 \left(b_{xi}^2 + Bi_x^2 + Bi_x\right)} = 1 - S_S. \tag{4.21}$$

The same can be also true about the infinite cylinder (Vergnaud, 1993):

$$\left(\frac{M}{M_\infty}\right)_{IC} = 1 - \sum_{i=1}^{\infty} \frac{4Bi_r^2 \exp\left(-b_{ri}^2 t_{nr}\right)}{b_{ri}^2 \left(b_{ri}^2 + Bi_r^2\right)} = 1 - S_{IC}. \tag{4.22}$$

Product solution for a finite cylinder is (Incropera *et al.*, 2017):

$$\left(\frac{M}{M_\infty}\right) = \left(\frac{M}{M_\infty}\right)_S + \left(\frac{M}{M_\infty}\right)_{IC} \left[1 - \left(\frac{M}{M_\infty}\right)_S\right] = 1 - S_S S_{IC}. \tag{4.23}$$

Combining Equations 4.22, 4.21, and 4.23:

$$\left(\frac{M}{M_\infty}\right) = 1 - \sum_{i=1}^{\infty} \frac{4Bi_r^2 \exp(-b_{ri}^2 t_{nr})}{b_{ri}^2 (b_{ri}^2 + Bi_r^2)} \sum_{j=1}^{\infty} \frac{2Bi_x^2 \exp\left(-b_{xj}^2 t_{nx}\right)}{b_{xj}^2 \left(b_{xj}^2 + Bi_x^2 + Bi_x\right)}. \tag{4.24}$$

This equation can be used to fit the parameter obtained in the AI passive release.

4.3.2 Monolith without membrane

In this case, the new partition coefficient (K) is between the monolith and the air (Figure 4.1):

$$K = \frac{C_1}{C_2}. \tag{4.25}$$

This means that:

$$K = \frac{K_2}{K_1}. \tag{4.26}$$

Where transfer rate is only Equation 4.4 and using Equation 4.25 the following equations can be written for the x,r, and C_n:

$$J_x = \frac{k_{m_x} A_x}{K} \left(C\left(t, H, r\right) - K\, C_\infty\right) \tag{4.27a}$$

$$J_r = \frac{k_{m_r} A_x}{K} \left(C\left(t, x, R_1\right) - K\, C_\infty\right) \tag{4.27b}$$

$$C_n = \frac{C\left(t, x, r\right) - K\, C_\infty}{C_0 - K\, C_\infty} = C_{n_S} C_{n_{IC}}. \tag{4.27c}$$

They are also solved with the same boundary conditions 4.13a to 4.13d but the Bi_r and Bi_x are:

$$Bi_x = \frac{k_{m_x} H}{K\, D} \tag{4.28a}$$

$$Bi_r = \frac{k_{m_r} R_1}{K\, D}. \tag{4.28b}$$

Equation 4.24 is still used but the Biot numbers are given by Equations 4.28a and 4.28b.

4.3.3 Limit solution for negligible external resistant

If the Biot number is big enough (Bi >100 (Çengel and Ghajar, 2015)) then can be used the solution for Biot $\to \infty$. Thus, Equation 4.24 is now (Siepmann and Siepmann, 2012):

$$\left(\frac{M}{M_\infty}\right) = 1 - \frac{32}{\pi^2} \sum_{i=1}^{\infty} \frac{\exp\left(-\pi^2 \left(2i-1\right)^2 t_{nx}/4\right)}{\left(2i-1\right)^2} \sum_{j=1}^{\infty} \frac{\exp\left(-b_{rj}^2 t_{nr}\right)}{b_{rj}^2} \tag{4.29}$$

where b_{rj} are the roots of Equation 4.30:

$$J_0\left(b_{rj}\right) = 0. \tag{4.30}$$

4.3.4 Monolith with membrane and negligible air resistance

If the air resistance is negligible when compared with the membrane resistance, then $\frac{L_M}{D_M} >> \frac{K_2}{k_{m_r}}$ and Biot number (Bi) is now written as:

$$Bi_x = \frac{P_{mem}H}{D} \tag{4.31a}$$

$$Bi_r = \frac{P_{mem}R_1}{D} \tag{4.31b}$$

with membrane permeability (P_{mem}) $(\mathrm{m} \cdot \mathrm{s}^{-1})$

$$P_{mem} = \frac{D_M \alpha_1}{L_M}. \tag{4.32}$$

Equation 4.24 is still used but the Biot numbers are given by Equations 4.31b and 4.31a.

4.3.5 Regimes

Considering the release caused by two regimes, one fraction of volatile (α_r) that can be released easily and a second fraction ($1 - \alpha_r$) where the release rate is very hard (Figure 3.3), thus can be considered as unreleased in a useful time and negligible.

$$\left(\frac{M}{\alpha_r M_\infty}\right) = 1 - S_S S_{IC}. \tag{4.33}$$

Where $S_S S_{IC}$ are given by Equations 4.21 and 4.22, respectively.

4.4 Model II: Active ingredient dispersion in a wind tunnel

The present section will develop a mathematical model for the dispersion of an AI in a tunnel with cylindrical coordinates. The AI is released from a disc placed in the middle of the tunnel with a radius equal to δR_2, as shown in Figure 4.3.

Considering a mass balance, to the AI in the wind tunnel and with its initial and boundary conditions (Hwang, 2021):

$$\frac{\partial C}{\partial t} + u\frac{\partial C}{\partial z} = D_z\frac{\partial^2 C}{\partial z^2} + D_r\left(\frac{\partial^2 C}{\partial r^2} + \frac{1}{r}\,\frac{\partial C}{\partial r}\right) \tag{4.34a}$$

$$C(0, z, r) = 0 \tag{4.34b}$$

$$\left.\frac{\partial C}{\partial z}\right|_{z=L} = 0 \tag{4.34c}$$

$$\left.\frac{\partial C}{\partial r}\right|_{r=0} = 0 \tag{4.34d}$$

$$\left.\frac{\partial C}{\partial z}\right|_{r=R_2} = 0 \tag{4.34e}$$

where:

$C(t, z, r)$ is the IA concentration in a given position ($\mathrm{kg} \cdot \mathrm{m}^{-3}$);

D_r is radial dispersion coefficient ($\mathrm{m} \cdot \mathrm{s}^{-1}$);

D_z is longitudinal dispersion coefficient ($\mathrm{m} \cdot \mathrm{s}^{-1}$).

The fourth condition for $z = 0$ will be now deducted, considering a macroscopic mass balance, of AI:

Accumulation= in - out

$$-Q = 0 + D_z \frac{dC}{dz} A_i - u_i A_i c \tag{4.35a}$$

$$\frac{Q}{\pi (R_2)^2} = u\, C\,(t, 0, r) - D_z \left.\frac{\partial C}{\partial z}\right|_{z=0}. \tag{4.35b}$$

Since the AI is only released in a small fraction of the R_2 (δ) [Equation 4.3] Equation 4.35b is more correctly written as:

$$\frac{Q\mathcal{H}\,(\delta R_2 - r)}{\pi (R_2 \delta)^2} = u\, C\,(t, 0, r) - D_z \left.\frac{\partial C}{\partial z}\right|_{z=0} \tag{4.36}$$

where $\mathcal{H}$ is the Heaviside step function.

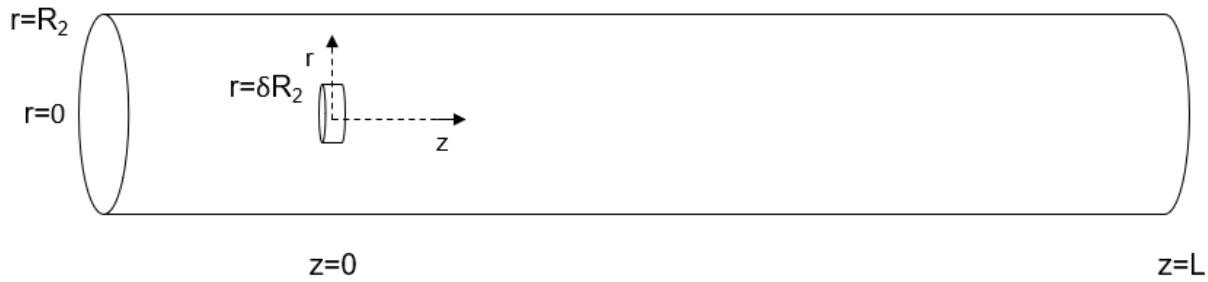

Figure 4.3: Sketch of the wind tunnel in cylindrical coordinates.

With the following normalized variable:

$$t_n = \frac{ut}{L} \tag{4.37a}$$

$$C_n = \frac{C}{c_{z0}} \tag{4.37b}$$

$$z_n = \frac{z}{L} \tag{4.37c}$$

$$r_n = \frac{r}{R_2} \tag{4.37d}$$

$$\alpha = \frac{D_z}{Lu} \tag{4.37e}$$

$$\beta = \frac{D_r L}{R_2^2 u} \tag{4.37f}$$

where:

α is scaled longitudinal dispersion coefficient;

β is a scaled radial dispersion coefficient.

With:

$$c_{z0} = \frac{Q}{\pi (R_2)^2}. \tag{4.38}$$

Equation 4.34a and its boundary condition now become:

$$\frac{\partial C_n}{\partial t_n} + \frac{\partial C_n}{\partial z_n} = \alpha \frac{\partial^2 C_n}{\partial z_n^2} + \beta \left(\frac{\partial^2 C_n}{\partial r_n^2} + \frac{1}{r_n} \frac{\partial C_n}{\partial r_n} \right) \tag{4.39a}$$

$$C_n(0, z_n, r_n) = 0 \tag{4.39b}$$

$$\left. \frac{\partial C_n}{\partial z_n} \right|_{z_n=1} = 0 \tag{4.39c}$$

$$\left. \frac{\partial C_n}{\partial r_n} \right|_{r_n=0} = 0 \tag{4.39d}$$

$$\left. \frac{\partial C_n}{\partial z_n} \right|_{r_n=1} = 0 \tag{4.39e}$$

$$\frac{\mathcal{H}(\delta - r_n)}{\delta^2} = C_n(t_n, 0, r_n) - \alpha \left. \frac{\partial C_n}{\partial z_n} \right|_{z_n=0}. \tag{4.39f}$$

To use the method of separation of variables, the following simplification was done to avoid the term $\frac{\partial C_n}{\partial z_n}$.

$$\phi = C_n \exp\left(-\frac{z_n}{2\alpha}\right). \tag{4.40}$$

Equation 4.39a becomes:

$$\frac{\partial \phi}{\partial t_n} + \frac{\phi}{4\alpha} = \alpha \frac{\partial^2 \phi}{\partial z_n^2} + \beta \left(\frac{\partial^2 \phi}{\partial r_n^2} + \frac{1}{r_n} \frac{\partial \phi}{\partial r_n} \right) \tag{4.41}$$

Considering $\phi_1 (z_n, r_n)$ the steady-state solution to Equation 4.41, with its boundary conditions, can be now written as:

$$\frac{\phi_1}{4\alpha} = \alpha \frac{\partial^2 \phi_1}{\partial z_n^2} + \beta \left(\frac{\partial^2 \phi_1}{\partial r_n^2} + \frac{1}{r_n} \frac{\partial \phi_1}{\partial r_n} \right) \tag{4.42a}$$

$$\left. \frac{\partial \phi_1}{\partial z_n} \right|_{z=1} + \frac{\phi_1 (1, r_n)}{2\alpha} = 0 \tag{4.42b}$$

$$\left. \frac{\partial \phi_1}{\partial r_n} \right|_{r_n=0} = 0 \tag{4.42c}$$

$$\left. \frac{\partial \phi_1}{\partial z_n} \right|_{r_n=1} = 0 \tag{4.42d}$$

$$\frac{\mathcal{H} (\delta - r_n)}{\delta^2} = \phi_1 (0, r_n) - \alpha \left. \frac{\partial \phi_1}{\partial z_n} \right|_{z_n=0}. \tag{4.42e}$$

The method of Separation Variable (Myint-U and Debnath, 2007) presuppose that ϕ_1 can be described as a function of z_n (F) and function of r_n (G).

If:

$$\phi_1 = AB; \tag{4.43}$$

then Equation 4.42a can be rewritten as:

$$\frac{AB}{4\alpha} = \alpha B \frac{\partial^2 A}{\partial z_n^2} + \beta A \left(\frac{\partial^2 B}{\partial r_n^2} + \frac{1}{r_n} \frac{\partial B}{\partial r_n} \right) \tag{4.44a}$$

$$\frac{1}{4\alpha\beta} - \frac{\alpha}{\beta A} \frac{\partial^2 A}{\partial z_n^2} = \frac{1}{B} \left(\frac{\partial^2 B}{\partial r_n^2} + \frac{1}{r_n} \frac{\partial B}{\partial r_n} \right) \tag{4.44b}$$

$$H(z_n) = G(r_n) \tag{4.44c}$$

Since z_n and r_n are independent variables, functions H and G must both be equal to a constant. Many constants may exist satisfying the equation H=G. Further, the constant must be negative since the boundary conditions in the r_n direction are homogeneous (Jiji, 2009). Thus, one writes:

$$H_i\left(z_n\right) = G_i\left(r_n\right) = -c_{1i}^2\,, \forall\ i \in \mathbb{N}. \tag{4.45}$$

Which represent two sets of Ordinary Differential Equations (ODEs). The case of a constant equal to zero must also be considered. The constants c_{1i} are designated as eigenvalues or characteristic values (Jiji, 2009).

The first ODE is:

$$H(z_n) = -c_{1i}^2 \tag{4.46a}$$

$$\frac{1}{4\alpha\beta} - \frac{\alpha}{\beta A_i}\frac{\partial^2 A_i}{\partial z_n^2} = -c_{1i}^2 \tag{4.46b}$$

$$\frac{1}{A_i}\frac{\partial^2 A_i}{\partial z_n^2} = -c_{2i}^2 \tag{4.46c}$$

$$c_{2i}^2 = \left(c_{1i}^2 + \frac{1}{4\alpha\beta}\right)\ \frac{\beta}{\alpha}\ . \tag{4.46d}$$

Of which solution is (Jiji, 2009):

$$A_i\left(z_n\right) = c_{3i}\exp\left(c_{2i}z_n\right) + c_{4i}\exp\left(-c_{2i}z_n\right)\ , \forall\ i \in \mathbb{N}. \tag{4.47}$$

For the special case of $c_{1i} = 0$, one has:

$$c_{20}^2 = \frac{1}{4\alpha^2}. \tag{4.48}$$

Equation 4.46b is now

$$\frac{1}{A_i}\frac{\partial^2 A_i}{\partial z_n^2} = -c_{20}^2. \tag{4.49}$$

Of which solution is (Jiji, 2009):

$$A_0\left(z_n\right) = c_{30}\exp\left(c_{20}z_n\right) + c_{40}\exp\left(-c_{20}z_n\right)\ . \tag{4.50}$$

The second set of ODEs is:

$$\frac{1}{B_i}\left(\frac{\partial^2 B_i}{\partial r_n^2}+\frac{1}{r_n}\frac{\partial B_i}{\partial r_n}\right)=-c_{1i}^2, \forall\ i\in\mathbb{N}. \tag{4.51}$$

Of which solution is (Jiji, 2009):

$$B_i\left(r_n\right)=c_{5i}J_0(c_{1i}r_n)+c_{6i}Y_0(c_{1i}r_n), \forall\ i\in\mathbb{N}_0. \tag{4.52}$$

For the special case of $c_{1i}=0$, one has, Equation 4.52 changes to:

$$B_0''+\frac{B_0'}{r_n}=0. \tag{4.53}$$

Of which solution is (Jiji, 2009):

$$B_0\left(r_n\right)=c_7+c_8\ln\left(r_n\right). \tag{4.54}$$

Since the original PDE in ϕ_1 (Equation 4.42a) is linear, the sum of all solutions for different values of c_{1i} are also a solution and the complete solution is thus (Jiji, 2009):

$$\phi_1\left(z_n,\ r_n\right)=A_0\left(z_n\right)B_0\left(r_n\right)+\sum_{i=1}^{\infty}A_i\left(z_n\right)B_i\left(r_n\right). \tag{4.55}$$

The constants c_3 to c_8 are now calculated from the boundary conditions.

$\phi_1\left(z_n,\ 0\right)$ is finite, since (Jiji, 2009):

$$\ln\left(0\right)=-\infty \tag{4.56a}$$

$$Y_0(0)=-\infty \tag{4.56b}$$

then:

$$c_{6i}=0 \tag{4.57a}$$

$$c_8=0. \tag{4.57b}$$

Boundary condition 4.42c can be solved into:

$$J_1(c_{1i})=0, \forall\ i\in\mathbb{N}. \tag{4.58}$$

Eigenvalues c_{1i} are then the zeros of the Bessel function $J_1(x)$ (except for $c_{1i}=0$). Boundary

condition 4.42d can be solved into:

$$c_{3i} = c_{4i}\frac{c_{2i} - c_{20}}{c_{2i} + c_{20}} \exp\left(-2c_{2i}\right), \forall\ i \in \mathbb{N}_0. \tag{4.59}$$

Therefore:

$$A_i\left(z_n\right) = c_{4i} \exp\left(-c_{2i} z_n\right) + \frac{c_{2i} - c_{20}}{c_{2i} + c_{20}} \exp\left(-c_{2i}(2 - z_n)\right) = c_{4i} E(c_{2i},\ z_n), \forall\ i \in \mathbb{N}_0 \tag{4.60}$$

$$E\left(c_{2i},\ z_n\right) = \exp\left(-c_{2i} z_n\right) + \frac{c_{2i} - c_{20}}{c_{2i} + c_{20}} \exp\left(-c_{2i}(2 - z_n)\right). \tag{4.61}$$

In this case, the complete solution is thus:

$$\phi_1\left(z_n,\ r_n\right) = c_9 E(c_{20},\ z_n) + \sum_{i=1}^{\infty} c_{10i} E(c_{2i},\ z_n) J_0(c_{1i} r_n). \tag{4.62}$$

Boundary 4.42e and using Equation 4.63 can be written as Equation 4.64:

$$F\left(c_{2i},\ 0\right) = \frac{E\left(c_{2i}, 0\right)}{2} - \alpha \left.\frac{\partial E}{\partial z_n}\right|_{z_n = 0} \tag{4.63}$$

$$c_9 F\left(c_{20},\ 0\right) + \sum_{i=1}^{\infty} c_{10i} J_0(c_{1i} r_n) F\left(c_{2i},\ 0\right) = \frac{\mathcal{H}\left(\delta - r_n\right)}{\delta^2}. \tag{4.64}$$

Multiplying both sides by $J_0(c_{1i} r_n) r_n$ into Equation 4.64 and integrating $\int_0^1 (.)\, dr_n$, one obtains (Jiji, 2009):

$$\int_0^1 c_9 F\left(c_{20},\ 0\right) J_0(c_{1i} r_n) r_n dr_n + \int_0^1 c_{10i} \left(J_0(c_{1i} r_n)\right)^2 F\left(c_{2i},\ 0\right) r_n dr_n = \int_0^1 \frac{\mathcal{H}\left(\delta - r_n\right)}{\delta^2} J_0(c_{1i} r_n) r_n dr_n \tag{4.65}$$

since (Jiji, 2009):

$$\int_0^1 J_0(c_{1i} r_n) r_n dr_n = J_1(c_{1i}). \tag{4.66}$$

Because of Equation 4.58, this is equal to zero.

$$\int_0^1 c_{10i} \left(J_0(c_{1i} r_n)\right)^2 F\left(c_{2i},\ 0\right) dr_n = \frac{(c_{1i} 1)^2 - 0^2}{2\ {c_{1i}}^2} \left(J_0(c_{1i} 1)\right)^2 \tag{4.67}$$

$$\int_0^1 \frac{\mathcal{H}\left(\delta - r_n\right)}{\delta^2} J_0(c_{1i} r_n) r_n dr_n = \frac{1}{\delta^2} \int_0^{\delta} J_0(c_{1i} r_n) r_n dr_n. \tag{4.68}$$

So, Equation 4.65 can be written as:

$$\frac{c_{10i}}{2} J_0^2\left(c_{1i}\right) F\left(c_{2i},\ 0\right) = \frac{J_1(c_{1i}\delta)}{c_{1i}\delta}. \tag{4.69}$$

Therefore:

$$c_{10i} = \frac{2J_1(c_{1i}\delta)}{F\left(c_{2i},\ 0\right) J_0^2\left(c_{1i}\right) c_{1i}\delta}\ . \tag{4.70}$$

Multiplying both sides by r_n into Equation 4.64 and integrating $\int_0^1 (.)\, dr_n$, one obtains (Jiji, 2009):

$$\int_0^1 c_9 F\left(c_{20},\ 0\right) r_n dr_n + \int_0^1 c_{10i} J_0(c_{1i} r_n) F\left(c_{2i},\ 0\right) r_n dr_n = \int_0^1 \frac{\mathcal{H}\left(\delta - r_n\right)}{\delta^2} r_n dr_n \tag{4.71}$$

Due to Equation 4.66:

$$\int_0^1 c_{10i} J_0(c_{1i} r_n) F\left(c_{2i},\ 0\right) r_n dr_n = 0 \tag{4.72}$$

For this case, Equation 4.71 is written as:

$$c_9 = \frac{1}{F\left(c_{20},\ 0\right)}. \tag{4.73}$$

Then Equation 4.62 can be written as:

$$\phi_1\left(z_n, r_n\right) = \frac{E(c_{20}, z_n)}{F\left(c_{20},\ 0\right)} + \sum_{i=1}^{\infty} \frac{2E(c_{2i}, z_n) J_0(c_{1i} r_n) J_1(c_{1i}\delta)}{F\left(c_{2i},\ 0\right) J_0^2\left(c_{1i}\right) c_{1i}\delta} \tag{4.74}$$

where E, F, α, β, c_{20}, and c_{2i} are functions present in Equations 4.61, 4.63, 4.37e, 4.37f, 4.48, and 4.46d, respectively.

c_{c1i} are the roots of Equation 4.58.

$$C_n(z_n, r_n) = \phi_1\left(z_n, r_n\right) \exp\left(\frac{z_n}{2\alpha}\right). \tag{4.75}$$

Numerical problems may arise in Equation 4.75 because the value of ϕ_1 may tend towards zero, and the value of the exponential may tend towards infinite. To avoid this, Equation 4.76 should be applied instead.

$$C_n(z_n, r_n) = 1 + \sum_{i=1}^{\infty} \frac{2E(c_{2i}, z_n) J_0(c_{1i} r_n) J_1(c_{1i}\delta)}{F\left(c_{2i},\ 0\right) J_0^2\left(c_{1i}\right) c_{1i}\delta} \tag{4.76}$$

where:

$$E(c_{2i}, z_n) = \exp(z_n\,(c_{20} - c_{2i})) + \frac{c_{2i} - c_{20}}{c_{20} + c_{2i}} \exp(z_n\,(c_{20} - c_{2i}) - 2c_{2i}) \tag{4.77a}$$

$$F(c_{2i}, 0) = \frac{1}{2} + \alpha c_{2i} + \frac{c_{2i} - c_{20}}{c_{20} + c_{2i}} \exp(2c_{2i})(\frac{1}{2} - \alpha c_{2i}) \tag{4.77b}$$

where α, β, c_{20}, and c_{2i} are present in Equations 4.37e, 4.37f, 4.48, and 4.46d, respectively.

c_{c1i} are the roots of Equation 4.58.

Combining with Equations 4.76, 4.38, in steady-state and with a Q constant in the middle of the tunnel ($r = 0$), the concentration in ($\mathrm{kg} \cdot \mathrm{m}^{-3}$) can be given by:

$$C_2(z, r) = \frac{Q\, C_n(z_n, r_n)}{u\pi R_2^2} \tag{4.78}$$

4.5 Model I + II: Active ingredient release from the monolith followed by dispersion in a wind tunnel

The release from the cylindrical monolith takes several days, and the time to reach steady-state in the wind tunnel transport is only a few minutes then is a good approximation to consider a pseudo-steady-state for the transport along the tunnel.

4.5.1 Internal diffusion

Figure 4.4 presents a sketch of the monolith.

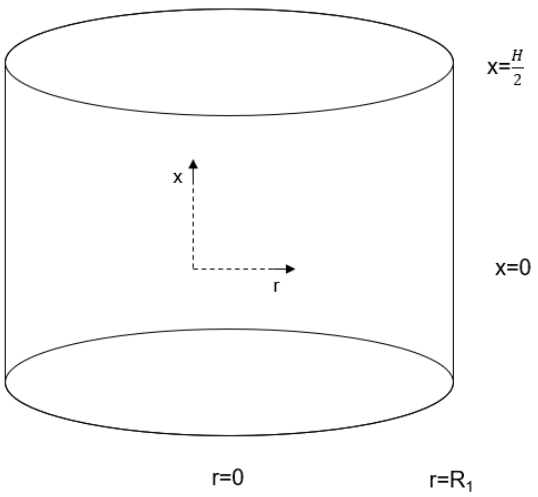

Figure 4.4: Sketch of the monolith.

The boundary conditions of the Equation 4.1a are now:

$$C\,(0, x, r) = C_0 \tag{4.79a}$$

$$\left.\frac{\partial C}{\partial r}\right|_{r=0} = 0 \tag{4.79b}$$

$$\left.\frac{\partial C}{\partial x}\right|_{x=0} = 0 \tag{4.79c}$$

$$-D\left.\frac{\partial C}{\partial x}\right|_{x=\frac{H}{2}} = k_x(K_1 C(t, \frac{H}{2}, r) - K_2 C_\infty) \tag{4.79d}$$

$$-D\left.\frac{\partial C}{\partial r}\right|_{r=R_1} = k_r(K_1 C(t, x, R_1) - K_2 C_\infty) \tag{4.79e}$$

Comparing the boundary conditions (4.1c) to (4.1f) with the previews conditions it is possible to see that the boundary condition are the same only that in section 4.3 it is considered the total height(H) of the monolith and in this section only half of the height($\frac{H}{2}$). In conclusion, the equations developed in Section 4.3 are used in this section, the only thing that changes is that H in the previous section is now $\frac{H}{2}$.

4.5.2 Dispersion in the tunnel

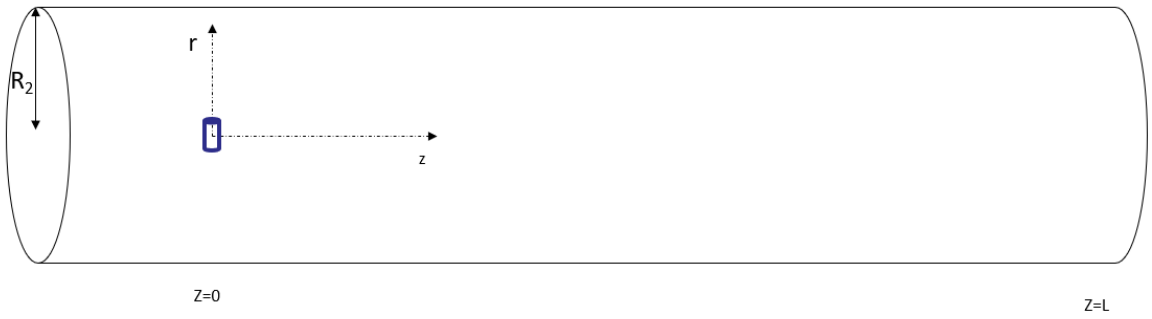

Figure 4.5: Sketch of the wind tunnel in cylindrical coordinates and with a monolith in it.

Comparing Figures 4.3 and 4.5 is possible to see that in this section the source of AI is a monolith, but in Section 4.4 is a disc, which is an approximation for the problem to be axisymmetric.

There is a small problem because the disc and the monolith do not have the same dimension, however, it was considered a disc with the same area as the surface area of the cylinder projected in a plane perpendicular to the z-direction.

$$\pi\,(\delta R_2)^2 = 2\,R_1 H \tag{4.80}$$

meaning:

$$\delta = \sqrt{\frac{2\,R_1 H}{\pi\,R_2^2}}. \tag{4.81}$$

4.5.3 Transition between models

The overall transport model is then the transient equations for the release from the cylinder (Equation 4.17), coupled with the steady-state solution in the wind tunnel for each time t (Equation 4.78).

The boundary condition linking the two models must relate C_∞ with C.

Analysing Figure 4.3, the transition must occur in the following conditions:

$$0 < r_i < \delta R_2 \ \wedge \ z = 0 \tag{4.82}$$

For this case, one has:

$$C_\infty\,(t) = C_2\,(0, r_i, t)\,\frac{Q(t)\phi_1\,(0, r_i)}{u\pi R_2^2} \tag{4.83}$$

If the value chosen for r_i is in the middle of the interval (Equation 4.85) then Equation 4.83 can be rewritten as:

$$C_\infty\,(t) = C_2\,(0, \delta R_2/2, t) = \frac{Q(t)\phi_1\,(0, \delta/2)}{u\pi R_2^2}. \tag{4.84}$$

$$r_i = \frac{\delta R_2}{2} \tag{4.85}$$

Solving this equation with Equation 4.17 (for a monolith with a membrane in a wind tunnel), one obtains:

$$Q\,(t) = \frac{C_0 K_1}{\frac{1}{k(t)} + \frac{\alpha_2\phi_1(0,\delta/2)}{u\pi R_2^2}} \tag{4.86}$$

with:

$$k(t) = (k_r f_r A_r K_1 \ + k_x f_r A_x K_1) \tag{4.87}$$

where ϕ_1, f_r, and f_x are given by Equation 4.74 4.18b and 4.18a.

The model inputs are $C_0; L_M; R_1; H; D; k_{m_x}; k_{m_r}; R_2; L; u; D_z; D_r; K_1$ and K_2.

In the case without membrane Equation 4.86 is now:

$$Q\,(t) = \frac{C_0/K}{\frac{1}{k(t)} + \frac{\phi_1(0,\delta/2)}{u\pi R_2^2}}\ . \tag{4.88}$$

with:

$$k(t) = \left(k_{m_r} f_r A_r K_1 \ + k_{m_x} f_r A_x K_1\right) \tag{4.89}$$

The model inputs are $C_0; R_1; H; D; k_{m_x}; k_{m_r}; R_2; L; u; D_z; D_r$ and K.

Chapter 5

Parameters estimation

5.1 Active ingredient dispersion coefficients

Active ingredient dispersion coefficients can be obtained using the theory present in Taylor (1954).

The velocity near the monolith (u_{star}) ($\mathrm{m} \cdot \mathrm{s}^{-1}$) (Taylor, 1954):

$$u_{star} = \sqrt{\frac{\tau}{\rho}} \tag{5.1}$$

where τ is the shear stress.

Considering the definition of friction coefficient (c_f):

$$c_f = \frac{2\tau}{\rho u^2} \tag{5.2}$$

so u_{star} are now (Taylor, 1954):

$$u_{star} = u\sqrt{\frac{c_f}{2}}. \tag{5.3}$$

Considering a turbulent regime with speed profiles, of temperature and concentrations completely established, and smooth tubes and $3 \times 10^3 < Re < 10^5$.

c_f can be obtained (Incropera *et al.*, 2017):

$$c_f = 0.079 Re^{-0.25}. \tag{5.4}$$

Reynolds number (Re) in the tunnel can be obtained using Equation 5.5 (where ρ and μ are density and dynamic viscosity of the fluid (air), respectively).

$$Re = \frac{2u\rho R_2}{\mu}. \tag{5.5}$$

For longitudinal dispersion considering effect due to longitudinal components of turbulent velocity and dispersion give (Taylor, 1954):

$$D_z = 10.1 R_2 u_{star} \tag{5.6a}$$

$$D_r = 0.064 R_2 u_{star}. \tag{5.6b}$$

5.2 Gas-Phase Diffusivity

According to Fuller's method, the diffusivity of a trace gas B in a bath gas A can be calculated by the following equation (Welty *et al.*, 2007):

$$D_{AB} = \frac{10^{-3} T^{1.75} \sqrt{\frac{1}{M_A} + \frac{1}{M_B}}}{P\left(\sqrt[3]{V_A} + \sqrt[3]{V_B}\right)^2} \tag{5.7}$$

where:

D_{AB} is the gas phase diffusivity of B in A ($\mathrm{cm}^2 \cdot \mathrm{s}^{-1}$);

T is the temperature (K);

P is the pressure (atm);

V_A and V_B are the dimensionless diffusion volumes of A and B, respectively.

The diffusion volume of a molecule (V) can be derived from the atomic diffusion volumes of atoms it contains present in reference (Welty *et al.*, 2007), and is given by Equation 5.8:

$$V = \sum_i^{n_i} V_i \tag{5.8}$$

where n_i is the number of the atom with a diffusion volume V_i.

To determine the values of k_{m_x} and k_{m_r} have used the definitions of the following dimensionless numbers: Reynolds (Re), Schmidt (S_c) and Sherwood (Sh) given by Equations 5.9, 5.10, 5.13, and 5.11 (Incropera *et al.*, 2017).

$$Re_x = \frac{2u\rho R_1}{\mu} \tag{5.9}$$

$$S_c = \frac{\mu}{\rho D_{AB}} \tag{5.10}$$

$$Sh_x = 0.664 Re_x^{\frac{1}{2}} S_c^{\frac{1}{3}} \tag{5.11}$$

$$k_{m_x} = 1.11284 \frac{Sh_x D_{AB}}{2R_1} \tag{5.12}$$

$$Sh_r = 0.683 Re_x^{0.466} S_c^{\frac{1}{3}} \tag{5.13}$$

$$k_{m_r} = \frac{Sh_r D_{AB}}{2R_1}. \tag{5.14}$$

5.3 Partition Coefficient

Strong negative deviations from Raoult´s law are observed in liquid mixtures where one component consists of very large molecules (polymers) and the other consists of molecules of normal size (Poling *et al.*, 2001).

The Flory–Huggins theory has long been the most prominent method for understanding the thermodynamics and phase behavior of polymer mixtures. The theory centers on the expression for free energy of mixing derived from a lattice model. The theory is constituted by combinatorial entropy terms associated with polymer chain configurations on the lattice, as well as an enthalpic contribution owing to interactions between the different species. The enthalpic term depends crucially on the Flory–Huggins interaction parameter (Young and Balsara, 2021).

For the present thesis, the monolith is considered a "solid solution", in which the polymer is the solvent and the small molecule is the solvent. The partition coefficient is going to be estimated using a modified Flory-Huggins.

$$\ln a = \ln \Phi_1 + (1 - \frac{1}{n})\Phi_2 + \chi\Phi_2^2 \tag{5.15a}$$

$$\Phi_1 = \frac{\frac{w_1}{\rho_1}}{\frac{w_1}{\rho_1} + \frac{w_2}{\rho_2}} \tag{5.15b}$$

$$\Phi_2 = \frac{\frac{w_2}{\rho_2}}{\frac{w_1}{\rho_1} + \frac{w_2}{\rho_2}} \tag{5.15c}$$

$$n = \frac{V_1^l}{V_2^l} \tag{5.15d}$$

where:

a is the activity (-);

χ is the Flory interaction parameter (-);

w_i is the weight fraction of component i (-);

Φ_i is the mass density (-);

M_i is the molar mass ($\mathrm{g \cdot mol^{-1}}$) of component i;

V_1^l and V_2^l is the molar volume of polymer (1) and solvent (2).

In typical polymer solutions $\frac{1}{n} << 1$(Poling *et al.*, 2001) so Equation 5.15a can be written as:

$$a = \Phi_1 \exp\left(\Phi_2 + \chi\Phi_2^2\right) \tag{5.16}$$

If K is the partition coefficient of an AI between a monolith (polymer) and air.

$$K = \frac{C_1}{C_2} \tag{5.17a}$$

With C_1 and C_2 being the concentration of the AI in the monolith and the air, as portrayed in Figure 4.1.

$$C_1 = \Phi_1 \rho_i \tag{5.17b}$$

$$C_2 = \frac{y_1 M_1 P}{RT} = \frac{a_1 P_1^\sigma M_1}{RT}. \tag{5.17c}$$

In conclusion,

$$K^{teo} = \frac{\rho_i RT}{P_1^\sigma M_1 \exp(\Phi_2 + \chi\Phi_2^2)} \tag{5.18}$$

$$K^{eff} = (1 - \epsilon)K^{teo} \tag{5.19}$$

where:

K^{teo} is the partition coefficient in the case of a non-porous monolith (-);

K^{eff} is the partition coefficient in the case of a porous monolith (-);

R is the gas constant ($\mathrm{J \cdot K^{-1} \cdot mol^{-1}}$);

P_1^σ is the vapor pressure of liquid AI (Pa);

ϵ is the porosity of the monolith (-).

If the value of the partition coefficient (K_A) for a given compound (A) is known, then it is possible to determine the value of the partition coefficient (K_B) for another compound (B), provided that the assumption that the mass density of the polymer (Φ_2) is approximately equal in both cases.

$$K_B = K_A \frac{\rho_B P_A^\sigma M_A}{\rho_A P_B^\sigma M_B} \exp(\Phi_2^2(\chi_A - \chi_B)). \tag{5.20}$$

Flory interaction parameter

The interaction parameter ($\chi_{1/2}$) can be estimated by using Hildebrand and Scott method (Equation 5.21) (Bansal *et al.*, 2016).

$$\chi_{1/2} = \frac{V_{M1} \left(\delta_{T1} - \delta_{T2}\right)^2}{RT} \tag{5.21}$$

with:

$$\delta_{T1}^2 = \delta_{D1}^2 + \delta_{P1}^2 + \delta_{H1}^2 \tag{5.22}$$

where:

V_{M1} is the molar volume of the solvent ($\mathrm{m}^3 \cdot \mathrm{mol}^{-1}$);

δ_{D1} and δ_{D2} is the Hansen solubility parameter for dispersion interactions of the solvent (1) and polymer (2) ($\mathrm{MPa}^{1/2}$);

δ_{P1} and δ_{P2} is the Hansen solubility parameter for polar interactions of the solvent (1) and polymer (2) ($\mathrm{MPa}^{1/2}$);

δ_{H1} and δ_{H2} is the Hansen solubility parameter for hydrogen bonding interactions of the solvent (1) and polymer (2) ($\mathrm{MPa}^{1/2}$);

δ_{T1} and δ_{T2} is the Hildebrand solubility parameter for interactions of the solvent (1) and polymer (2) ($\mathrm{MPa}^{1/2}$).

If the value of the Flory interaction ($\chi_{A/2}$) for a given compound (A) is known, then it is possible to determine the value of the Flory interaction ($\chi_{B/2}$) for another compound (B):

$$\chi_{B/2} = \chi_{A/2} \frac{V_{MB} \left(\delta_{TB} - \delta_{T2}\right)^2}{V_{MA} \left(\delta_{TA} - \delta_{T2}\right)^2}. \tag{5.23}$$

Chapter 6

Modeling simulation and parameter fitting

In cases where there are infinite sums (Equations 4.9a; 4.9b; 4.19a; 4.19b; 4.76; 4.29 and 4.24) values were evaluated to 4 digits which is good enough compared with the experimental errors (Figure 3.6).

The optimization objective is to reduce the Root Mean Squared Error (RMSE) (Equation 2.8).

In the wind tunnel experience given that, for the first time (that should be for 1 minute), there is an experimental error (Figure 3.6) and the objective of the product is to be useful for a long period, so it was used a weight of 0.1 this means:

$$RMSE = \sqrt{\frac{0.1(y_{exp1} - y_{mod1})^2 + \sum_{i=2}^{N}(y_{exp} - y_{mod})^2}{N}} \tag{6.1}$$

here:

y_{exp} is the experiential value (without first time);

y_{mod} is the value predicted with the model (without first time);

y_{exp1} is the experiential value for the first time;

y_{mod1} is the value predicted with the model for the first time;

N is the number of experiential points.

In both experiments was used the Particle Swarm Optimization (PSO) method and was used a pre-built *MATLAB R2021a* function *particleswarm* present in "Global Optimization Toolbox version 4.5" with the following options: use parallel computing ("Parallel Computing Toolbox version 7.4") in the way to use more than one core; a Function tolerance of 10^{-7} (The algorithm only stops when the value of the objective function between 2 consequent iterations is less than 10^{-7}) and a hybrid model (this means that after achieving the optimal point with the particle swarm can "refine" the result using a local solver). The parameters used in the PSO method are decided internally by the algorithm.

To avoid numerical problems, in the optimization process, all the variables were normalized ($x = x_0 \times x_i$) here x_0 is the initial guess, x_i is the optimization variable.

To find the roots (Equations 4.58, 4.30, 4.11a, and 4.11b) was used a pre-built-function *Find-Roots* present in "CharFunTool The Characteristic Functions Toolbox version 1.4.1." which estimates the real roots of an oscillatory function on the interval, by using an adaptive n-order Chebyshev polynomial approximation of the function (Witkovsky, 2021).

As mentioned in Section 4.2, the method used to determine the roots should be fast and accurate. To test the *FindRoots* method, the roots of Equation 4.58 were calculated using this approach. The results obtained were compared with the "(real values) or real plot". This comparison is represented in Figure 6.1, The *FindRoots* method was capable of finding 53 roots in just 0.05 s.

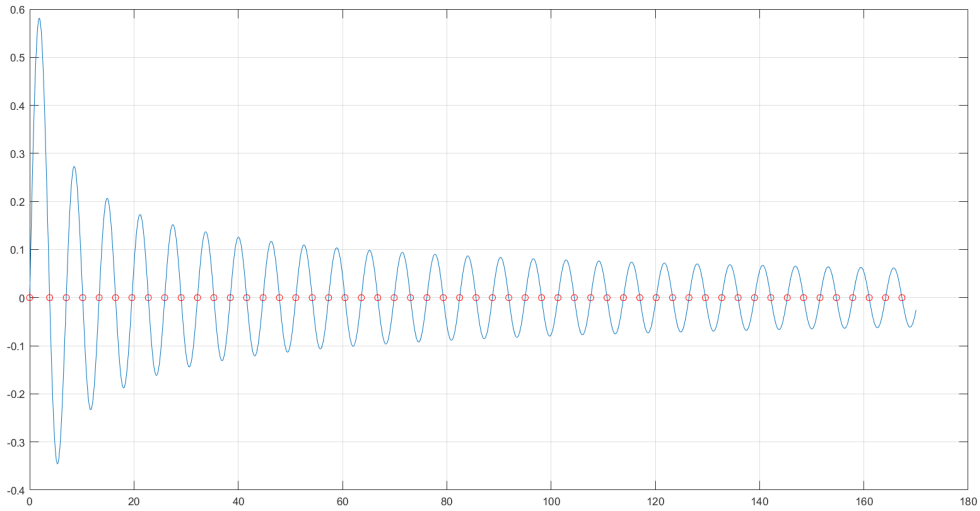

Figure 6.1: Roots of Equation 4.58 found by using the Chebyshev approximation.

Chapter 7

Results

7.1 Parameter estimation

Flory Huggins's theory was used to find the partition coefficient to a non-porous monolith ($K^{teo}_{\alpha-pinene/PLC}$). Firstly the theoretical Flory interaction for α-pinene ($\chi_{\alpha-pinene/PLC}$) was determined using Equation 5.21 and the value of $K^{teo}_{\alpha-pinene/PLC}$ was then obtained using Equation 5.18.

To find the mass transfer coefficient of the active ingredient (AI) in the air for r and x-direction (k_{m_r} and k_{m_x}) is necessary to determine the gas diffusivity of α-pinene in the air ($D_{air/\alpha-pinene}$) or eucalyptol in the air ($D_{air/eucalyptol}$) using Fuller's method present in Equation 5.7. Radial (D_{r0}) and longitudinal (D_{z0}) dispersion coefficients can be obtained using the theory present in Taylor (1954) and using Equations 5.6b and 5.6a.

Table 7.1 presents the values mentioned above, the physical and chemical properties of α-pinene, eucalyptol, and PLC are present in Appendix A. The values are for a mass density of 0.5 and a temperature of 20 °C.

Table 7.1: Parameters estimates.

Proprieties	Value
$\chi_{\alpha-pinene/PLC}$ (-)	0.550
$K^{teo}_{\alpha-pinene/PLC}$(-)	12856
$D_{air/\alpha-pinene} \times 10^6$ ($\mathrm{m}^2 \cdot \mathrm{s}^{-1}$)	5.95
$D_{air/eucalyptol} \times 10^6$ ($\mathrm{m}^2 \cdot \mathrm{s}^{-1}$)	5.76
$D_{z0} \times 10^2$ ($\mathrm{m}^2 \cdot \mathrm{s}^{-1}$)	4.4
$D_{r0} \times 10^4$ ($\mathrm{m}^2 \cdot \mathrm{s}^{-1}$)	2.79

The theoretical value for the partition coefficient to a porous (K) monolith is distinct to the different experiences and is determined using Equation 5.19. Also, for each experience, the

value of k_{m_x} and k_{m_r} are calculated. The data are present in Table 7.2.

Table 7.2: Parameters estimates that depend on the conditions of each experiment.

Experiment	$k_{m_x} \times 10^2$ $(\mathrm{m} \cdot \mathrm{s}^{-1})$	$k_{m_r} \times 10^3$ $(\mathrm{m} \cdot \mathrm{s}^{-1})$	K (-)
Exp1	1.19	8.4	2044
Exp2	1.19	8.4	2609
Exp3	1.14	8.4	2880
Exp4	1.14	8.4	3060
Exp5	1.19	8.4	2674
Exp7	1.15	8.5	-
Exp8	1.15	8.5	-
Exp9	1.15	8.5	-

7.2 Preliminary testing

Using Exp1 condition (manufacture conditions present in Table 3.1) as an example, and the above estimate of D_z0, Figure 7.1 shows that the value of D_z that minamizes the Root Mean Squared Error (RMSE) tends to be zero. The monolith creates a whirlwind around it, causing the profile of wind velocity more pug flow likely than expected. It will lead to a smaller longitudinal dispersion than predicted.

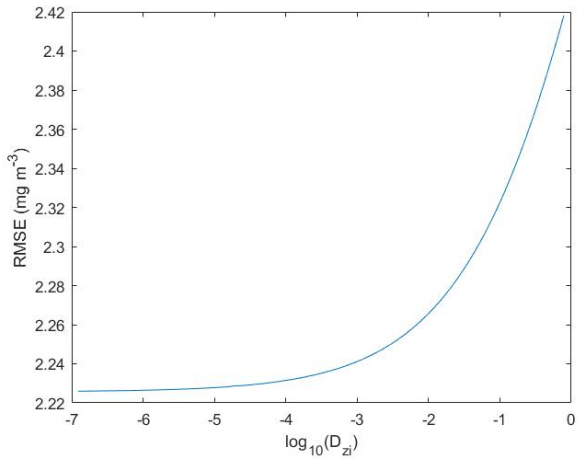

Figure 7.1: Effect of longitudinal dispersion (D_z) on $RMSE.D_{zi}$ is a normalized value equals to D_z/D_{z0}, with D_{z0} being the value in Table 7.1.

Analyzing Figure 7.1 it is possible to see that for values smaller than -4, the RSME does not vary much so, a virtual restriction for $D_{zi} \geqslant 10^{-2}$ $(\log \approx -4.60)$ is chosen.

To test the assumption of Section 4.3.5, Figure 7.2 with $\alpha_r = 1$ and compared with Figure 7.8a (present in Section 7.4) where α_r can be adjusted.

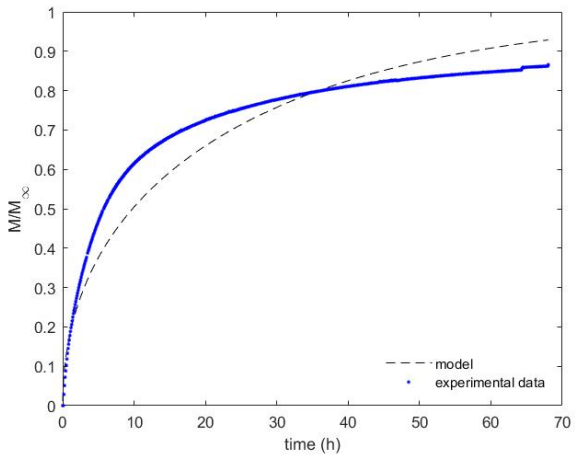

Figure 7.2: α-pinene release experimental fitting to Exp3 with $\alpha_r = 1$.

It is possible to see that the equation with α_r is a good approach.

Figure 7.3 evaluates the normalized concentration (ϕ_1) to the boundary condition for $z_n = 0$ to different values of r_i. It is possible to see that the value of ϕ_1(Equation 4.74) appears to have two regimes, one for $0 < r_i < \delta R_2$ (Equation 4.82), and the other to $\delta R_2 < r_i < R_2$. Figure 7.4 evaluates the concentration of the AI in the wind tunnel for the regime to position P1 of the tunnel. Exp1 was chosen to test this. The value δ (Equation 4.81) is 0.1281.

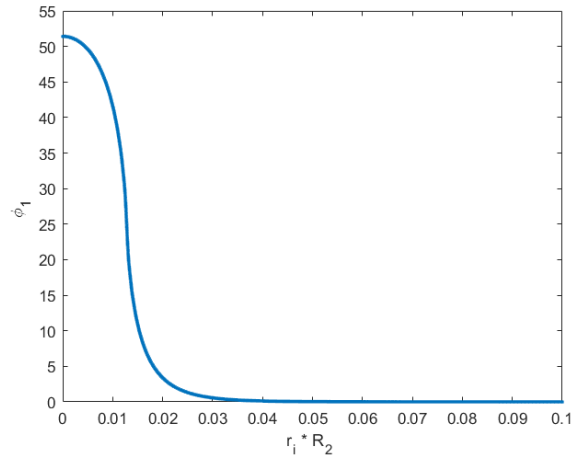

Figure 7.3: Value of $\phi_1(0, r_i)$ to different r_i.

In conclusion, for any value between 0 and δ, the error in the concentration is less than 1% and, thus negligible.

7.3 Illustrative example

The model that describes the diffusion internal followed by dispersion on the tunnel can predict the concentration for different spatial positions and time.

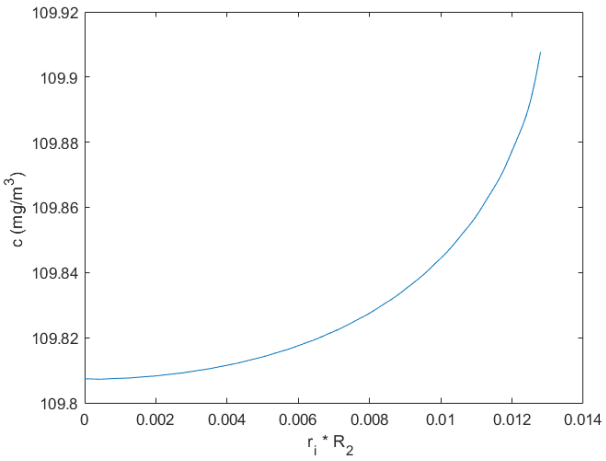

Figure 7.4: Concentration in a wind tunnel for different values of r_i.

As describe in Section 4.5, the tunnel is a pseudo-steady-state system, where the tunnel is in a steady state and the dynamic is given by the release from the monolith.

Using as an example the Exp1 and the parameter determined in Section 7.1, the value of the internal coefficient is the value present in Table 7.3. It is difficult to represent data in a 4D. Firstly, is considered a pseudo-steady-state after 1 h. The concentration of the AI (C) in that state for the tunnel for every radius position (r) and tunnel lengths (z), in Figure 7.5, is present a 3D chart for the entire tunnel.

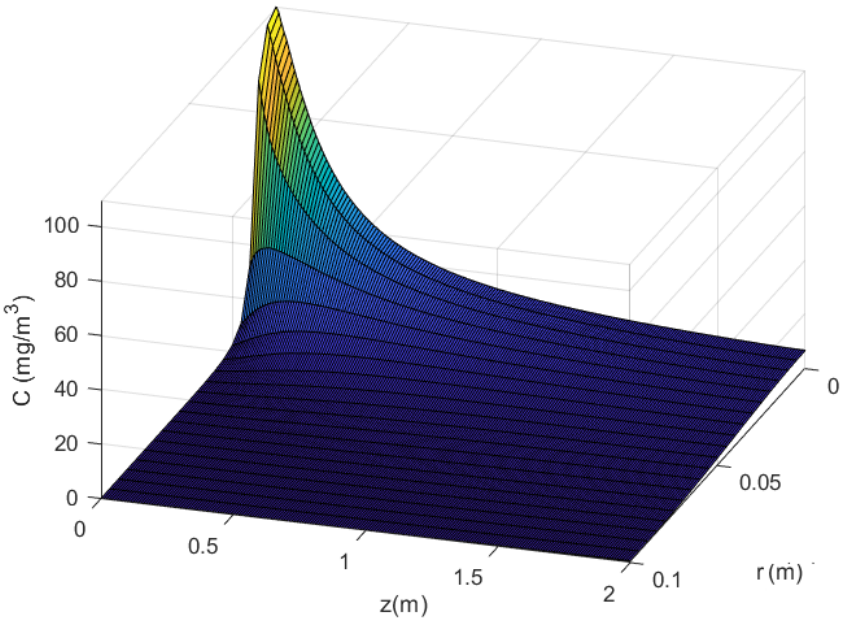

Figure 7.5: 3 D representation of the concentration along the tunnel in a pseudo-steady-state.

Figure 7.6 presents the predicted concentration of the AI along the tunnel length for different values of r between 0 and 0.1 m.

Considering $r_2 = 0$ m as built a 2D plot with the concentration as a function of time and z, and

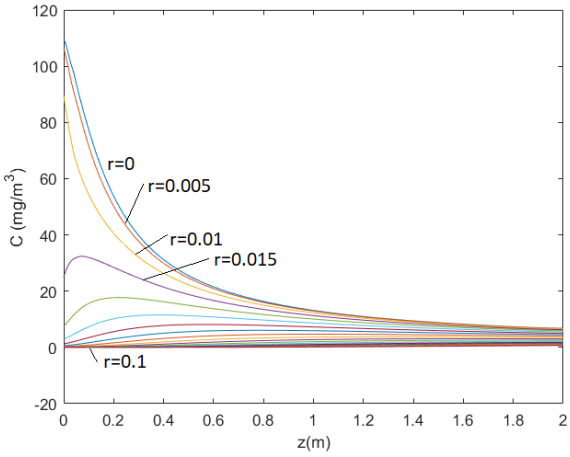

Figure 7.6: AI concentration along the tunnel in a pseudo-steady-state for different radial positions.

are present in Figure 7.7. In appendix B is present the 3D Figure for this case.

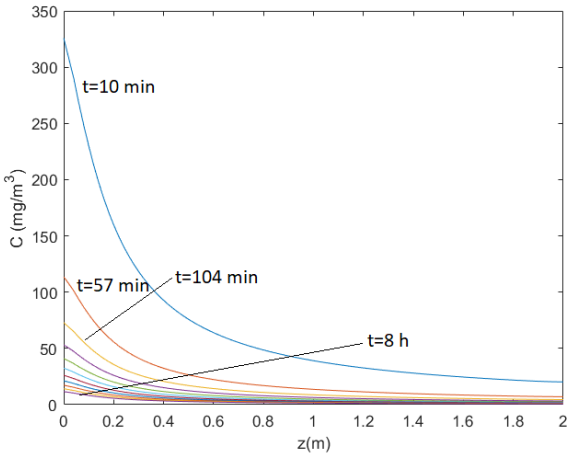

Figure 7.7: AI concentration in the centre of the tunnel for various times between 10 min and 8h.

7.4 Fitting results

The experiences used in this section (Exp1 to Exp10) have different manufacturing conditions (present in Table 3.1).

For the first experience (AI passive release), the model used is model I (develop in Chapter 4), and all the experiences were used to adjust the model parameters.

For the second experience (AI release and dispersion in a wind tunnel), the model used is model I + II (develop in Chapter 4), and the experiences Exp1 to Exp5 (with α-pinene) were used to adjust the parameters and the Exp7 to Exp9 (with eucalyptol) were used in a predictive way and compared with the experimental data to test the predictive capacity.

7.4.1 Active ingredient passive release

Absence of membrane

Bernardo *et al.* (2019) show that Biot number tends towards ∞, so the first approach is the start with this consideration thus using Equation 4.29 it is possible to adjust the data to find the effective internal diffusion coefficient (D), the fraction of volatile that can be released in a useful time (α_r) and, the RMSE, and are present in Table 7.3. The model fitting to Exp1 and Exp2 was previously conducted in Bernardo *et al.* (2019).

Table 7.3: Model fitting results: active ingredient release without membrane.

Experiment	D $\times 10^{10}$ ($m^2 \cdot s^{-1}$)	α_r(-)	RMSE (-)
Exp1	7.15±2.00	1.00±0.00	0.015–0.016
Exp2	1.06±0.02	1.00±0.00	0.012–0.025
Exp3	1.59±0.79	0.86±0.02	0.0112–0.0147
Exp4	1.80±0.18	0.80±0.08	0.0069–0.0103
Exp5	1.08±0.35	0.87±0.04	0.0026–0.0069
Exp7	0.89±0.10	0.93±0.01	0.0088–0.0096
Exp8	1.21±0.26	0.91±0.03	0.0093–0.0159
Exp9	1.05±0.54	0.92±0.01	0.0068–0.0109

Figure 7.8 presents the model fitting to each of the replicas of experience Exp3. The results for the other experiences (Exp4, Exp5, and Exp7 to Exp9) are shown in Appendix C.

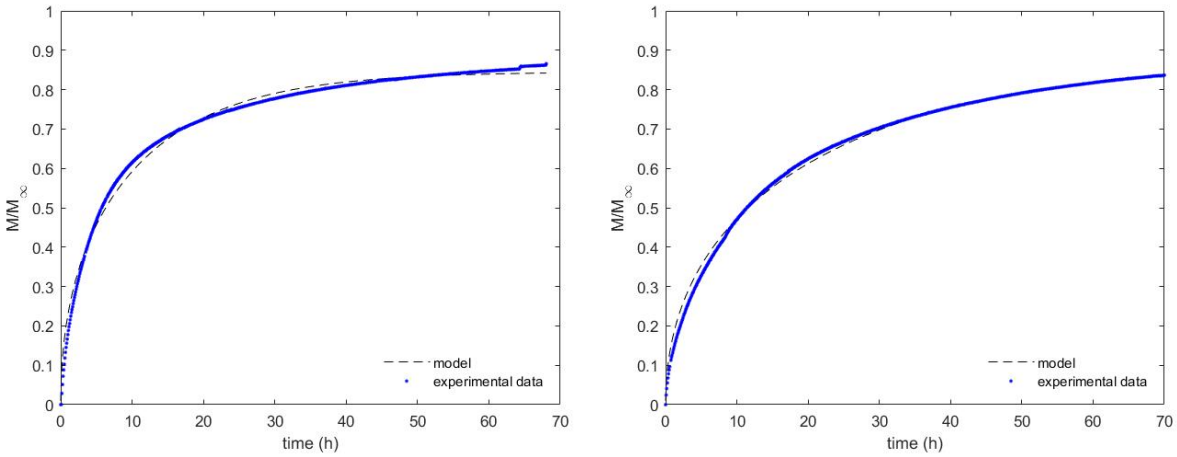

(a) Replica I **(b)** Replica II

Figure 7.8: α-pinene release model fitting to Exp3.

The release profile varies widely between the 2 replicas as can be seen in Figure 7.8 justifying the high value of the standard deviation when compared with the mean in the value of D (Table 7.3).

Biot number (Bi) represents the ratio between internal and external mass transfer resistances.

Bernardo *et al.* (2019) concluded that for Exp1 the Biot number tends to be ∞. In all the other experiences, the value of D is smaller than the value for Exp1. which means that the internal resistance is even bigger and thus, the value of Bi continues to tend to ∞.

With membrane

The production condition of Exp6 is the same as Exp1 (as can be seen in Table 3.1), then the internal values (D and α) are the same for both, the same conclusion can be said about Exp7 and Exp10.

As said before, the air resistance is negligible, using Equations 4.31a, 4.31b, and 4.24, and the information present in Table 7.3 it is possible to determine the membrane permeability (P_{mem}), and the values are present in Table 7.4

Table 7.4: Model fitting results: active ingredient release with membrane.

Experiment	$P_{mem} \times 10^{12}$ (m $\cdot$ s^{-1})	RMSE (-)
Exp6	2.57±0.26	0.0142–0.0156
Exp10	0.96±0.31	0.0234–0.0425

Figures 7.9 and 7.10 present the model fitting to each of the replicas of experiences Exp6 and Exp10, respectively.

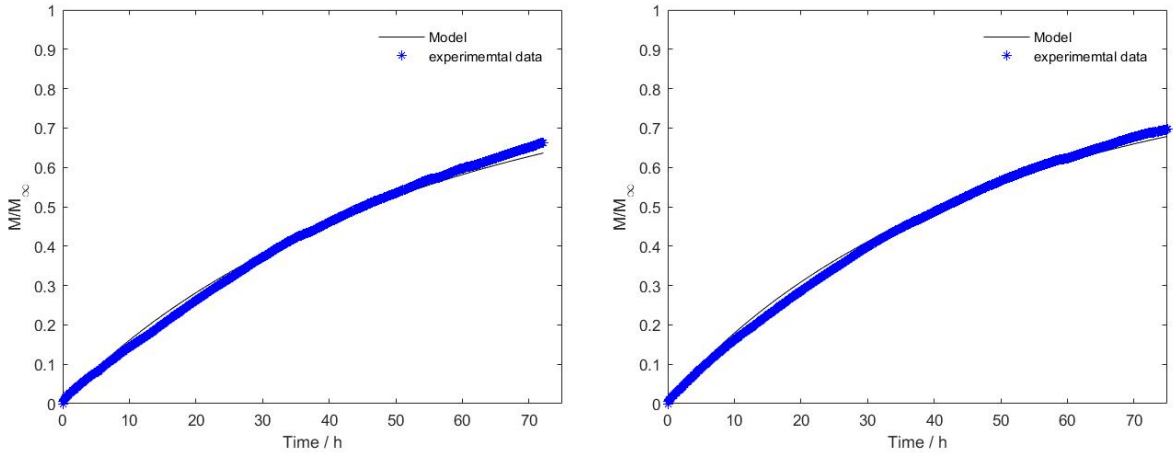

(a) Replica I **(b)** Replica II

Figure 7.9: Model fitting to Exp6 (α-pinene, membrane).

7.4.2 Active ingredient release and dispersion in a wind tunnel

Considering the average of wind velocity, effective internal coefficient (Table 7.3), and initial concentration of AI (Table 3.2) corrected with the value of α_r determined above (Table 7.3), and adjusting the experimental data can find the optimal parameter to each experience and present in Table 7.5.

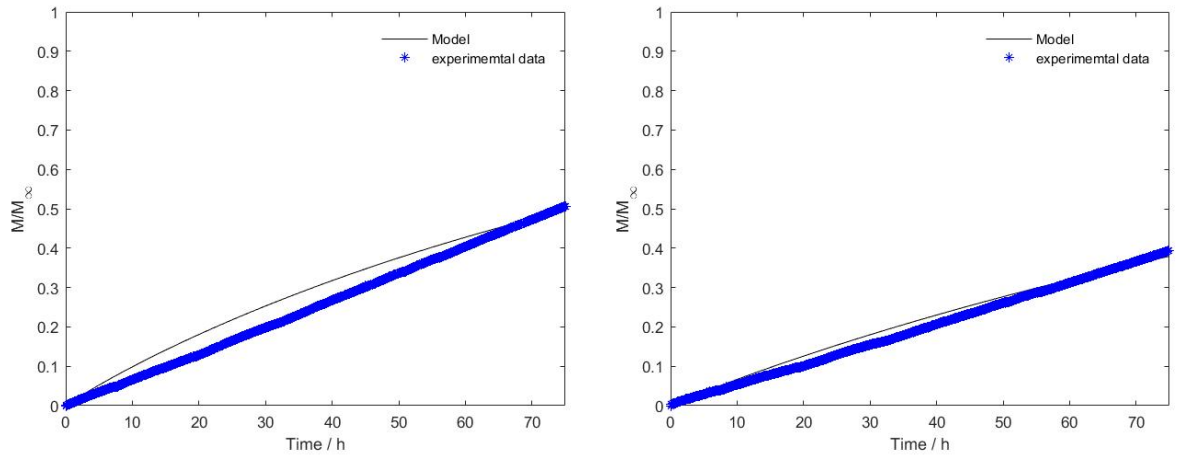

(a) Replica I **(b)** Replica II

Figure 7.10: Model fitting to Exp10 (Eucalyptol, membrane).

Table 7.5: Model fitting results: active ingredient transport in the wind tunnel.

Experiment	$D_z \times 10^4$ ($\mathrm{m}^2 \cdot \mathrm{s}^{-1}$)	$D_r \times 10^4$ ($\mathrm{m}^2 \cdot \mathrm{s}^{-1}$)	K (-)	RMSE($\mathrm{mg} \cdot \mathrm{m}^{-3}$)
Exp1	4.41	10.9	2772	2.6406
Exp2	4.41	7.30	134	3.3905
Exp3	4.41	2.66	1049	5.2246
Exp4	4.41	2.67	831	8.8871
Exp5	4.41	2.67	358	2.3542

The values of Table 7.5 are for the average of wind velocity (u), internal coefficient (D), and initial concentration (C_0), however, those parameters have a considerable effect on the concentration at each time. After a quick analysis, it is concluded that for a small velocity (u), great D and C_0 lead to larger values to the first instants. So Figures 7.11 to 7.15 are built with the experimental data, adjustment curve, curve with u equal to mean (x) plus standard deviation (σ), D and C_0 equal to $x - \sigma$ and another opposite.

As said before in Section 7.4.1, Exp3 and Exp6 are related. Using the values of D, α, D_z, D_r, from Exp3, and P from experience Exp6. in that case there is only one variable optimizable the partition coefficient air-membrane (K_2). However, the number of experiences is too low to have a statistical value, and therefore not used.

7.5 Prediction

Eucalyptol and α-pinene are similar in structure. and considering that the wind velocity is the same, therefore D_z and D_r are equal for α-pinene and eucalyptol.

Analysing Figures 7.11b and 7.12b, the AI concentration in the tunnel is greater than zero at point P_1'. The model predicts a value of AI concentration at point P_1' of almost 0 $\mathrm{mg} \cdot \mathrm{m}^{-3}$ for

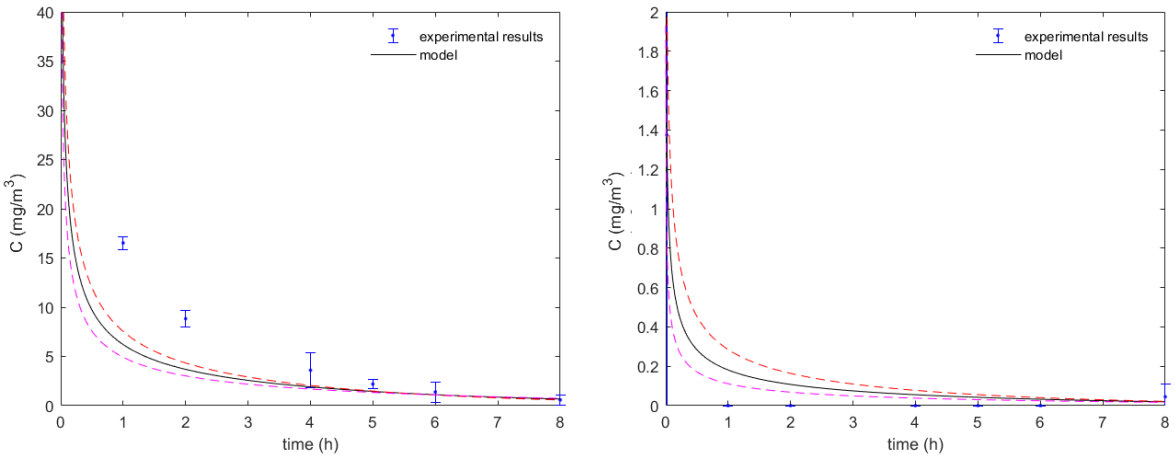

(a) Point P_1

(b) Point $P_1^{'}$

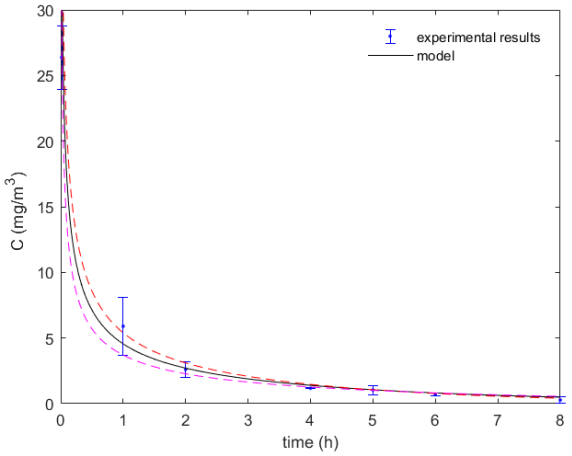

(c) Point P_2

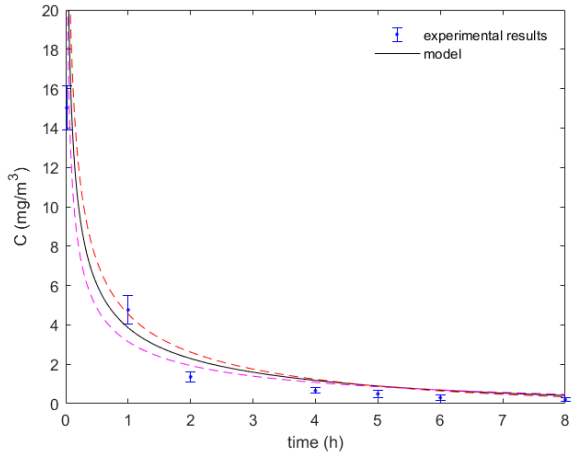

(d) Point P_3

Figure 7.11: Model fitting to experience Exp1 at different points in the tunnel.

the parameter fitted in experiences Exp3 to Exp5.

So in conclusion, the values of D_r for experiences Exp3 to Exp5 was not the correct one, and thus, D_r used is the values of Exp1 and Exp2.

The mean value of the experimental partition coefficient to a non-porous monolith PCL and α-pinene ($K^{exp}_{\alpha-pinene/PCL}$) with Equation 5.18 the value of Flory iteration ($\chi^{exp}_{\alpha-pinene/PCL}$) for the experimental data for the α-pinene ($\chi^{exp}_{\alpha-pinene/PCL}$), and the expected value of Flory iteration for eucalyptol ($\chi^{exp}_{eucalyptol/PCL}$) with Equation 5.23 and the expected value of the partition coefficient for the eucalyptol for the non-porous PCL ($K^{teo}_{eucalyptol/PCL}$) with Equation 5.20. Data are present in Table 7.6.

With Equation 5.19 it is possible to determine the coefficient to a porous cylinder (K) and the value of RSME for this perdition.As said in Section 7.4.2, the values of u, D and C_0 vary and were considering the same values, then Figures 7.16 to 7.18 were built.

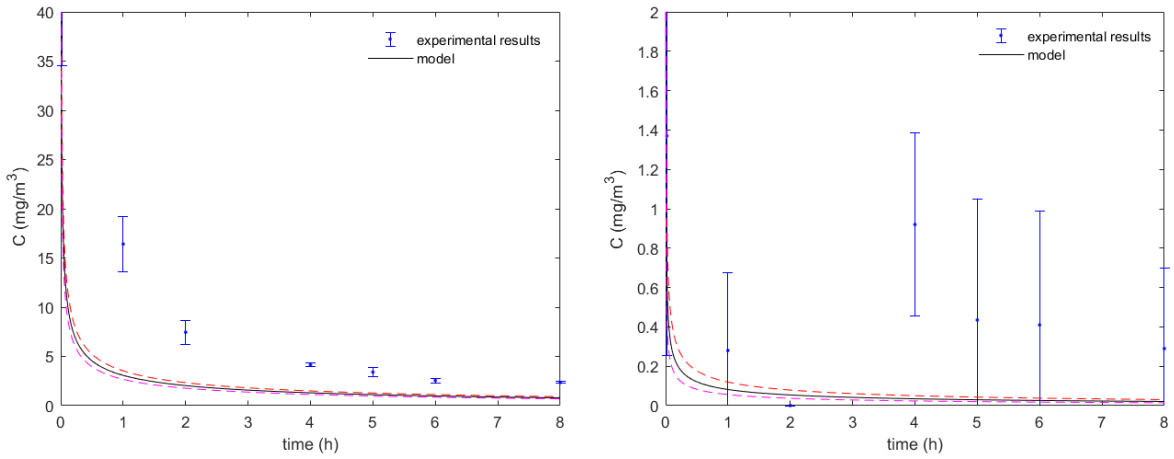

(a) Point P_1

(b) Point $P_1^{'}$

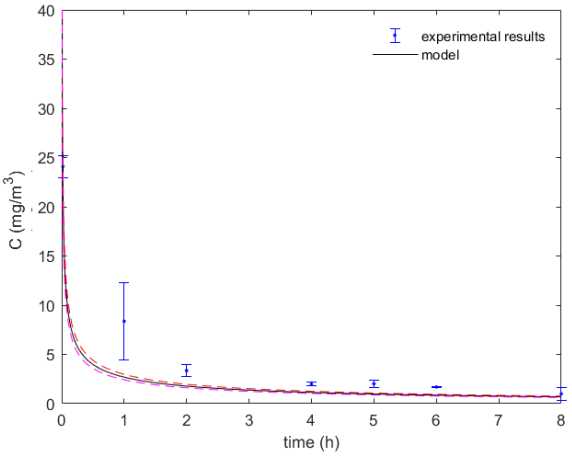

(c) Point P_2

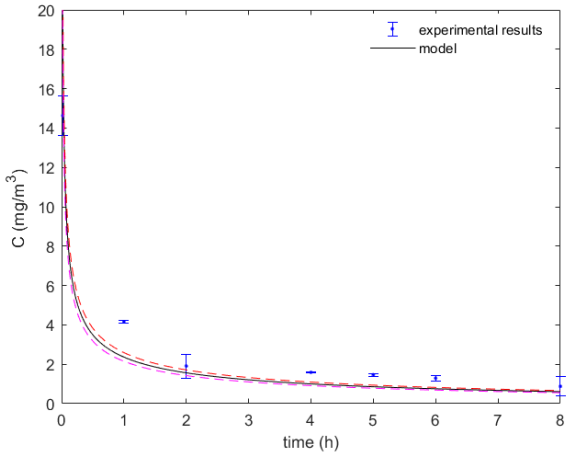

(d) Point P_3

Figure 7.12: Model fitting to experience Exp2 at different points in the tunnel.

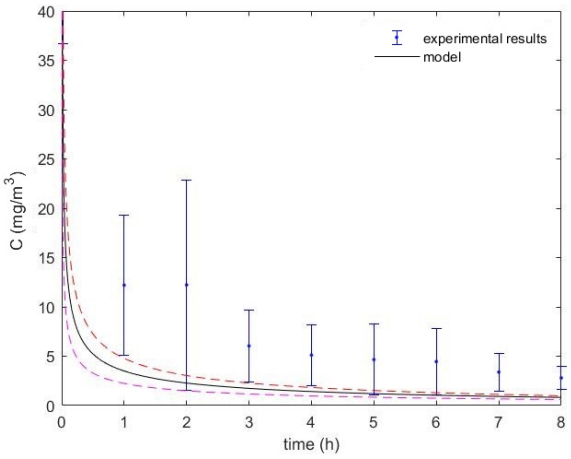

Figure 7.13: Model fitting to experience Exp3 at point P_3.

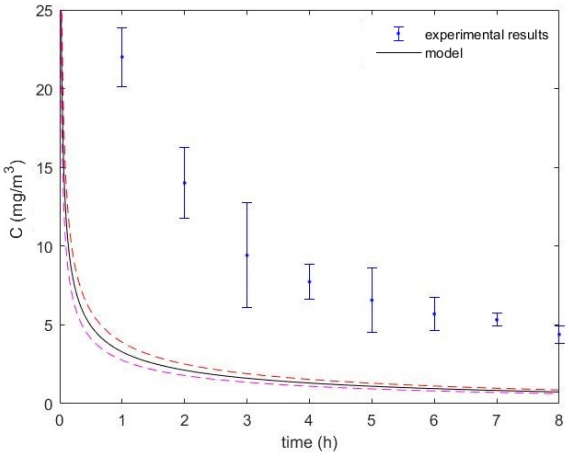

Figure 7.14: Model fitting to experience Exp4 at point P_3.

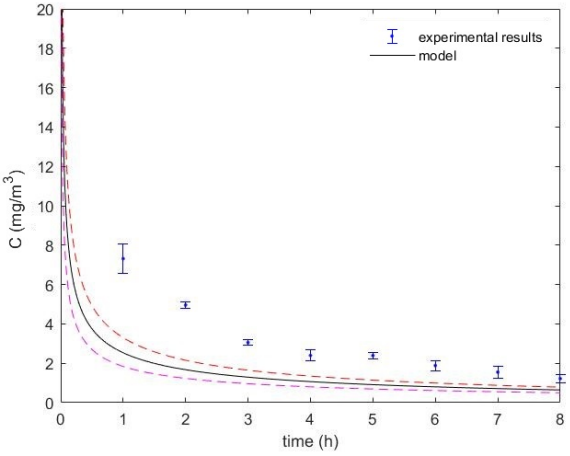

Figure 7.15: Model fitting to experience Exp5 at point P_3.

7.6 Subsequent analysis

The model for the wind tunnel describes the reality with a systematic error, causing the expected concentration (most of the time) to be lower than the real one. One possible explanation is that

Table 7.6: Dispersion coefficients and Flory Huggins parameters predicted values.

Proprieties	Value
$D_z \times 10^4$ ($\mathrm{m}^2 \cdot \mathrm{s}^{-1}$)	4.41
$D_r \times 10^4$ ($\mathrm{m}^2 \cdot \mathrm{s}^{-1}$)	9.1
$K^{exp}_{\alpha pinene/PCL}$ (-)	5598
$\chi^{exp}_{\alpha-pinene/PCL}$ (-)	3.94
$\chi^{exp}_{eucalyptol/PCL}$ (-)	2.44
$K^{teo}_{eucalyptol/PCL}$ (-)	19385

Table 7.7: Predicted partition coefficient.

Experiment	K (-)	RMSE (-)
Exp7	4109	5.6247
Exp8	4090	5.6845
Exp9	3858	7.3964

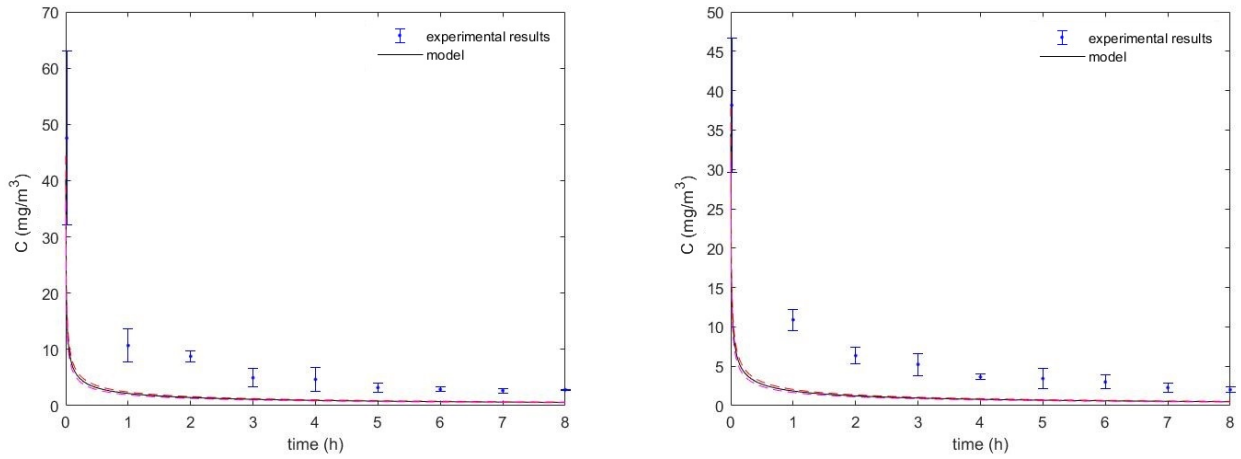

(a) **(b)**

Figure 7.16: Model prediction versus Exp7 results at different points in the tunnel.

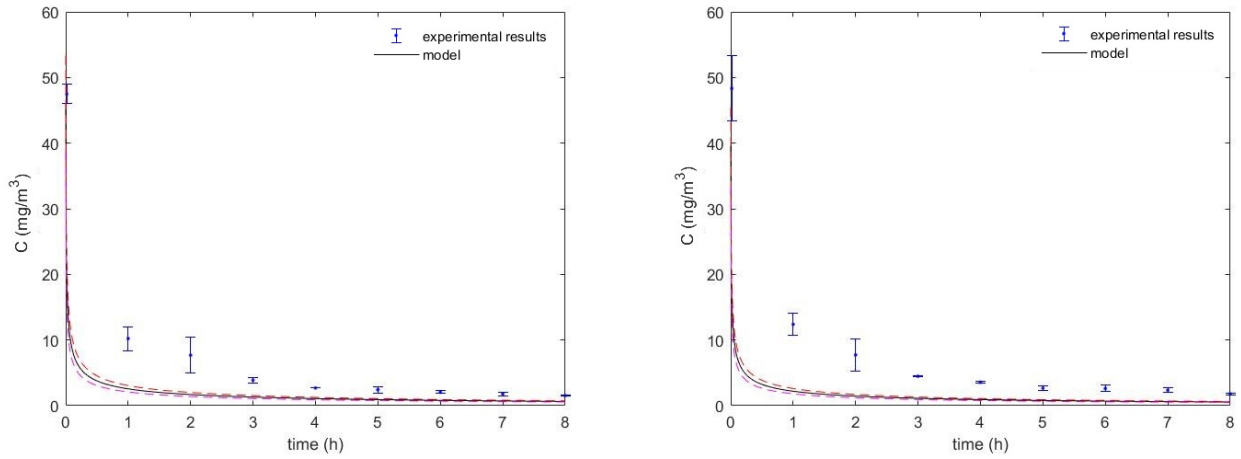

(a) Point P_2 **(b)** Point P_3

Figure 7.17: Model prediction versus Exp8 results at different points in the tunnel.

because the product is placed in a windy position (contrary to the AI release experience) the internal diffusion may not be passive release anymore, and thus value may be greater than the AI release test may suggest.

To test the effect of D on the results, two simulations are done, one with the "normal" value of "D" and a second one with a value of D ten times bigger than the normal. Figures 7.19 shows the results for the conditions of Exp2.

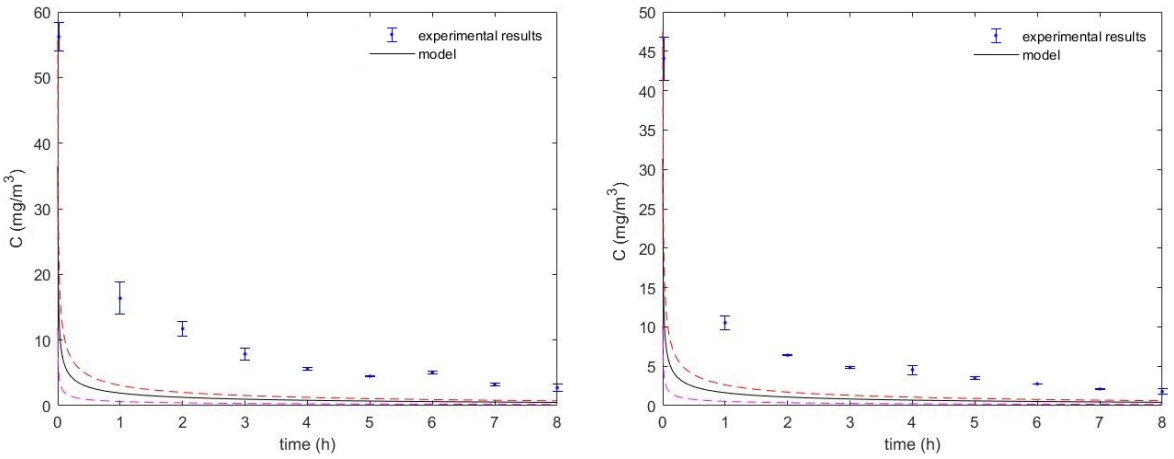

(a) Point P_2 **(b)** Point P_3

Figure 7.18: Model prediction versus Exp9 results at different points in the tunnel.

A higher value of D will lead to a higher concentration for the initial instant, but it leads to early exhaustion and hence lower concentration for later times. This means that the value of D is influential in the result but isn´t enough to explain the difference.

The partition coefficient between the PCL and the α-pinene is comprised between 134 and 2772, as seen in Table 7.5. To test the effect of the partition coefficient on AI concentration Figure 7.21 was built, with these two extreme values of K.

As can be seen in Figure 7.21, the two values of the partition coefficient do not have a visible impact on the concentration. One possible explanation for these results is that for these two cases the internal mass resistance is much greater than the external resistance.

As can be seen in Equations 4.14b and 4.14a for a bigger value of K can cause the increase of the external mass resistance. Figure 7.21 was built into the Exp2 with the partition coefficient of 124 (the "normal" value) and 5×10^4.

As could be seen in Figure 7.21, the value of the partition coefficient, after all, affects the result. Having into account Equation 5.18, the volatility of the AI and the interaction with the polymer is related to the partition coefficient. Therefore, the partition coefficient does not have a significant impact for compounds having volatility similar to the one of the α-pinene (or higher) and a similar affinity to the polymer. On the other hand, it has a significant impact, for compounds having lower volatility to the α-pinene and a similar affinity to the polymer.

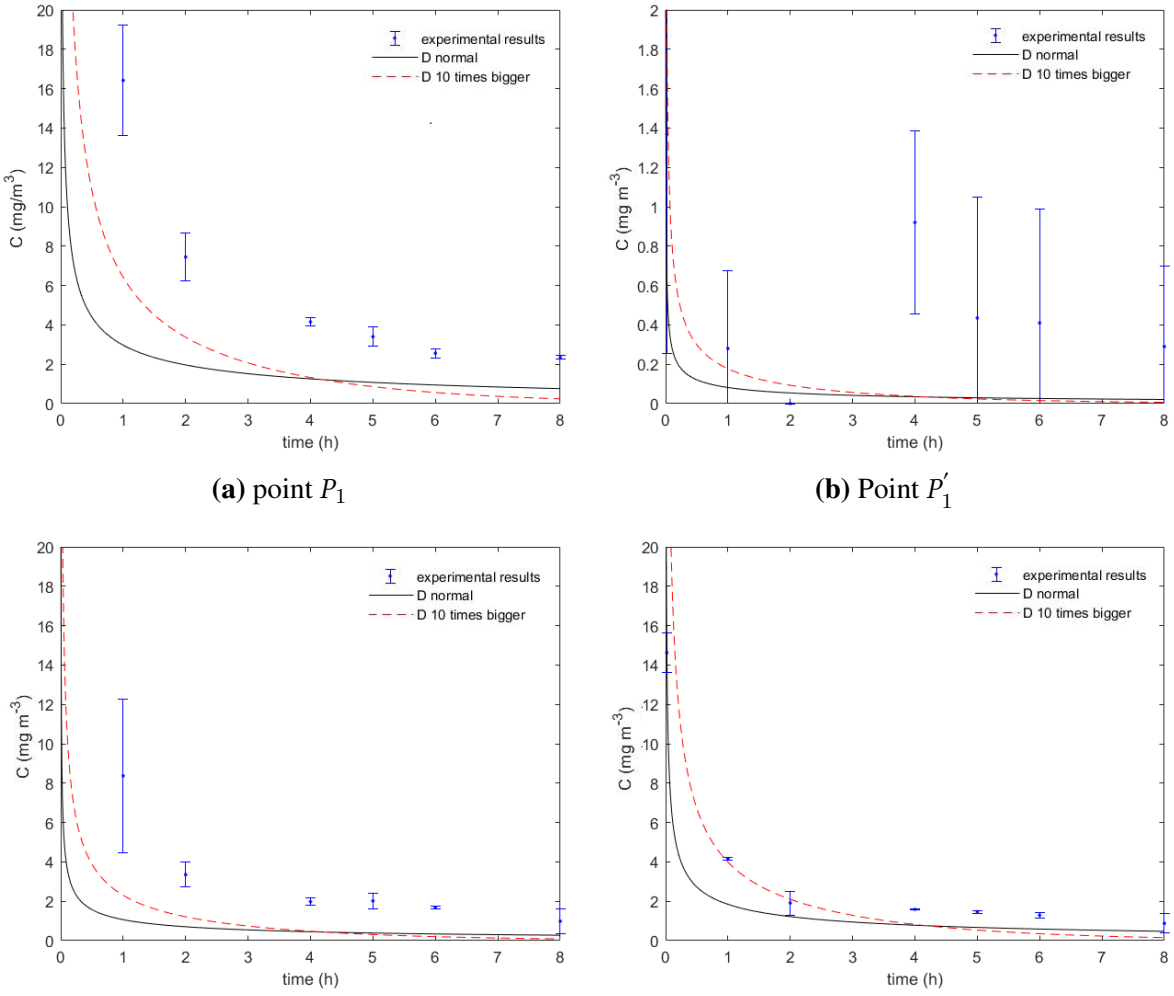

(a) point P_1

(b) Point P_1'

(c) Point P_2

(d) Point P_3

Figure 7.19: Effect of diffusion on AI concentration to Exp2 conditions.

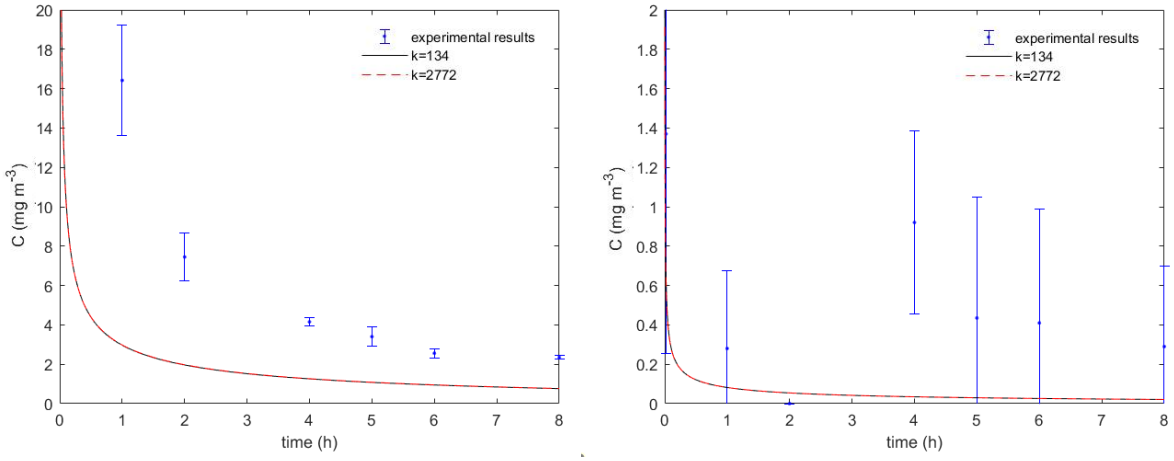

(a) Point P_1.

(b) Point $P_1^{'}$

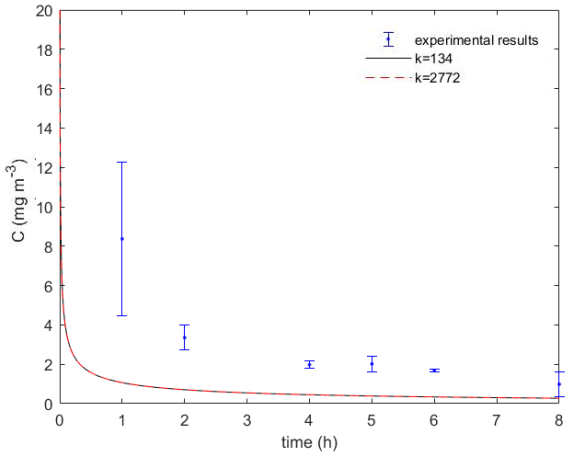

(c) Point P_2

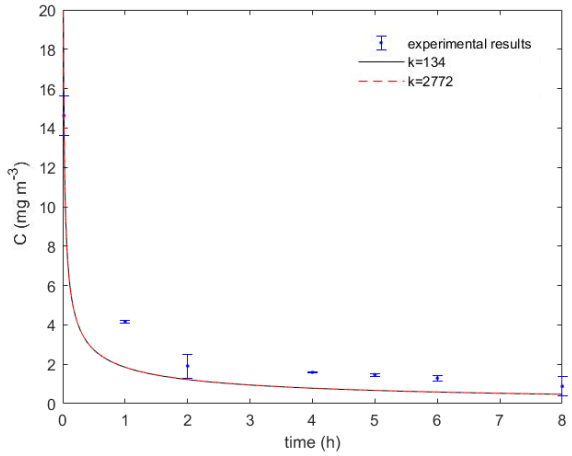

(d) Point P_3

Figure 7.20: Effect of the partition coefficient on AI concentration to Exp2 conditions.

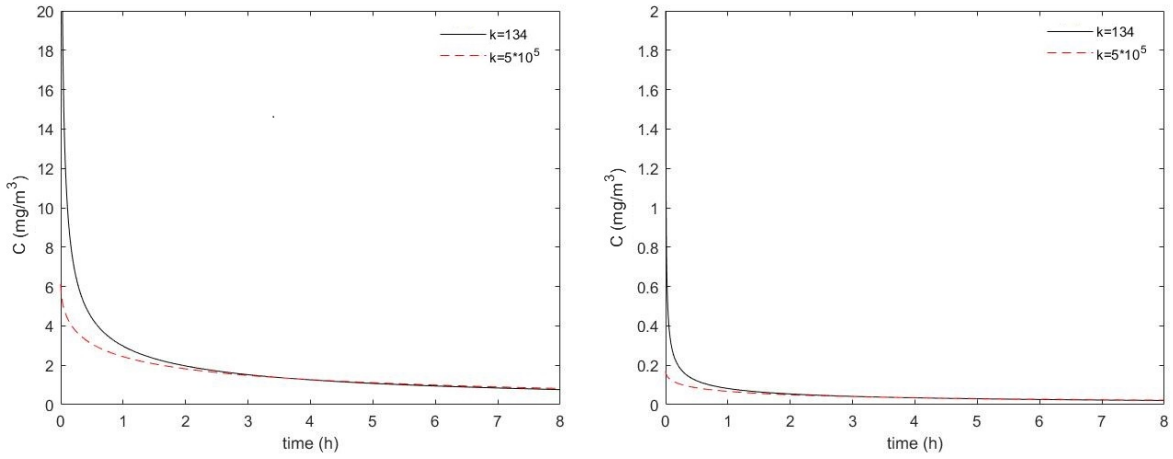

(a) Point P_1

(b) Point $P_1^{'}$

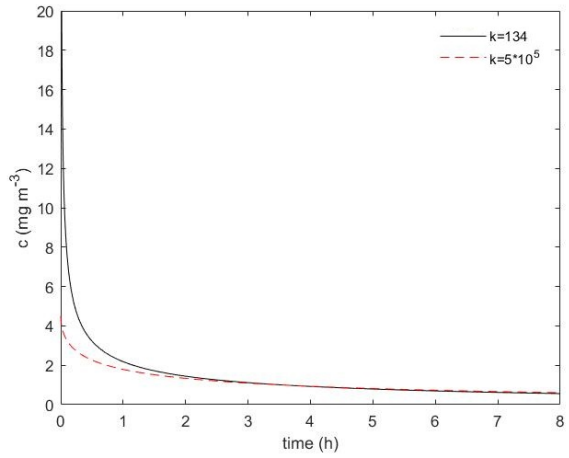

(c) Point P_2

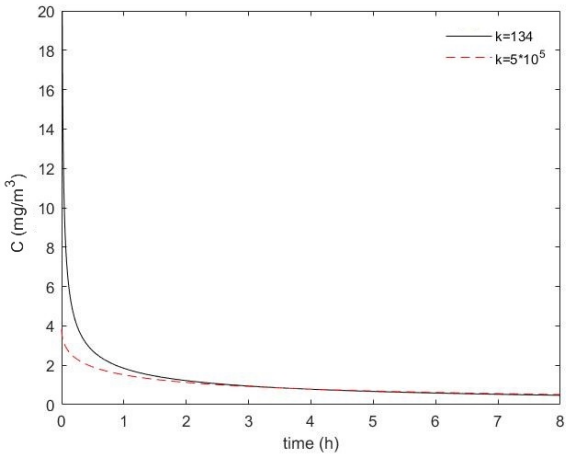

(d) Point P_3

Figure 7.21: Effect of the partition coefficient with the fitting value versus a higher value on AI concentration to Exp2 conditions.

Chapter 8

Conclusions and future work

For the active ingredient (AI) passive release test, the model developed predicts almost perfectly the results. However, the experimental repeatability is low (probably due to uncontrolled manufacturing factors).

In the AI release and dispersion in a wind tunnel test, the longitudinal dispersion coefficient is smaller than the theoretical due to the effect of the cylinder in the flow system. The partition coefficient does not have a significant impact on the concentration of the AI in the tunnel. Flory Huggins's theory is a good approximation to determine the partition coefficient.

The model has a systematic error. Nevertheless, this data seems to have a considerable experimental error. The model uncertainties are in the same order of magnitude as the experimental error. An experimental point to a different radius position (e.g., point $P_1^{'}$) should be used to determine the radial dispersion.

Despite this systematic error, analytical solutions are still useful because they can give a quicker answer, are helpful for the parameter fitting (it has less computational effort), also sensitivity analysis is easier compared with the numerical solution, also this model can be used in a way to improve the product function.

Some experiences were unexplored in the present thesis, such as with a mixture of some AIs and with the same manufacture conditions used in this thesis, but with a membrane. Those experiments could be used in future work.

Some model improvements can be done, such as using Computational Fluid Dynamics to better describe the gas flow in the tunnel, namely the effect of the monolith in the flow, and therefore produce more reliable predictions of the AI concentration at any point in the gase phase. On the other hand, the model for the AI release from the product may be upgraded to incorporate the effect of the monolith microstructure, and how that microstructure is in part determined by the manufacturing process conditions.

Chapter 9

Bibliography

Almeida, B. and Coppo Leite, V. (2019). *Particle Swarm Optimization: A Powerful Technique for Solving Engineering Problems*, chapter 3. IntechOpen.

Bansal, K., Baghel, U. S., and Kowalski, Thakral, S. (2016). Construction and validation of binary phase diagram for amorphous solid dispersion using flory–huggins. *AAPS PharmSciTech*, 17(23):318–327.

Batu, V. (1989). A generalized two-dimensional analytical solution for hydrodynamic dispersion in bounded media with the first-type boundary condition at the source. *Water Resources Research*, 25(6):1125–1132.

Batu, V. (1993). A generalized two-dimensional analytical solute transport model in bounded media for flux-type finite multiple sources. *Water Resources Research*, 29(8):2881–2892.

Batu, V. (1996). A generalized three-dimensional analytical solute transport model for multiple rectangular first-type sources. *Journal of Hydrology*, 174(1):57–82.

Bernardo, F., Braga, B., and Chim, R. (2019). A wind tunnel method to develop products for controlled delivery of volatiles: experimental apparatus and mathematical model. In *The 12th european congress of chemical engineering*.

Braga, M. (2020). Ecovector project. `http://www.prodeq.eu/content/ecovector`. Accessed: 2021-08-01.

Chen, J.-S., Chen, J.-T., Liu, C.-W., Liang, C.-P., and Lin, C.-W. (2011a). Analytical solutions to two-dimensional advection–dispersion equation in cylindrical coordinates in finite domain subject to first- and third-type inlet boundary conditions. *Journal of Hydrology*, 405(3):522–531.

Chen, J.-S., Liu, Y.-H., Liang, C.-P., Liu, C.-W., and Lin, C.-W. (2011b). Exact analytical solutions for two-dimensional advection–dispersion equation in cylindrical coordinates subject to third-type inlet boundary condition. *Advances in Water Resources*, 34(3):365–374.

Chen, X., Chen, M., Xu, C., and Yam, K. L. (2019). Critical review of controlled release packaging to improve food safety and quality. *Critical Reviews in Food Science and Nutrition*, 59(15):2386–2399. PMID: 29553807.

de Matos, M. B., Puga, A. M., Alvarez-Lorenzo, C., Concheiro, A., Braga, M. E., and de Sousa, H. C. (2015). Osteogenic poly(ϵ-caprolactone)/poloxamine homogeneous blends prepared by supercritical foaming. *International Journal of Pharmaceutics*, 479(1):11–22.

Dehghan, M. (2007). Time-splitting procedures for the solution of the two-dimensional transport equation. *Kybernetes*, 36:791–805.

Dominković, D., Ćosić, B., Bačelić Medić, Z., and Duić, N. (2015). A hybrid optimization model of biomass trigeneration system combined with pit thermal energy storage. *Energy Conversion and Management*, 104:90–99. Special Issue on Sustainable development of energy, water and environment systems.

Dominković, D. F., Ćosić, B., Medić, Z. B., and Duić, N. (2015). A hybrid optimization model of biomass trigeneration system combined with pit thermal energy storage. *Energy conversion and management*, 104:90–99.

Edgar, T., Himmelblau, D., and Lasdon, L. (2001). *Optimization of Chemical Processes*. McGraw-Hill, Boston, 1st edition.

Eftaxias, A., Font, J., Fortuny, A., Fabregat, A., and Stüber, F. (2002). Nonlinear kinetic parameter estimation using simulated annealing. *Computers and Chemical Engineering*, 26(12):1725–1733.

Çengel, Y. and Ghajar, A. (2015). *Heat and mass transfer: Fundamentals and applications*. McGraw-Hill Education, New York, NY, 5th edition.

Finlayson, B. (1980). *Nonlinear Analysis in Chemical Engineering*.

for Biotechnology Information, N. C. (2021a). Pubchem compound summary for cid 2758, eucalyptol. `https://pubchem.ncbi.nlm.nih.gov/compound/Eucalyptol`. Accessed: 2021-07-01.

for Biotechnology Information, N. C. (2021b). Pubchem compound summary for cid 6654, alpha-pinene. `https://pubchem.ncbi.nlm.nih.gov/compound/alpha-Pinene`. Accessed: 2021-07-01.

Goimil, L., Braga, M. E., Dias, A. M., Gómez-Amoza, J. L., Concheiro, A., Alvarez-Lorenzo, C., de Sousa, H. C., and García-González, C. A. (2017). Supercritical processing of starch aerogels and aerogel-loaded poly(ϵ-caprolactone) scaffolds for sustained release of ketoprofen for bone regeneration. *Journal of CO2 Utilization*, 18:237–249.

Hansen, C. (2012). *Hansen Solubility Parameters: A User's Handbook, 2nd Edition*.

Hutomo, G., Kusuma, J., Ribal, A., Mahie, A., and Aris, N. (2019). Numerical solution of 2-d advection-diffusion equation with variable coefficient using du-fort frankel method. *Journal of Physics: Conference Series*, 1180:012009.

Hwang, G. (2021). A unified approach to two-dimensional linear advection-dispersion equation in cylindrical coordinates on a finite domain. *International Journal of Heat and Mass Transfer*, 164:120569.

Incropera, F., Bergman, T. L., Lavine, A. S., and DeWitt, D. P. (2017). *Fundamentals of Heat and Mass Transfer.* Wiley's Enhanced, New York, NY, 5th edition.

Jiji, L. (2009). *Heat conduction*. Springer, New York, NY, 3rd edition.

Katsikadelis, J. T. (2002). *Boundary elements: theory and applications*. Elsevier.

Kennedy, J. and Eberhart, R. (1995). Particle swarm optimization. In *Proceedings of ICNN'95 - International Conference on Neural Networks*, volume 4, pages 1942–1948 vol.4.

Leij, F. J., Skaggs, T. H., and Van Genuchten, M. T. (1991). Analytical solutions for solute transport in three-dimensional semi-infinite porous media. *Water resources research*, 27(10):2719–2733.

Lian, G., Malone, m., and Homan, j. (2004). A mathematical model of volatile release in mouth from the dispersion of gelled emulsion particles. *Journal of Controlled Release*, 98(1):139–155.

Marseguerra, M., Zio, E., and Podofillini, L. (2003). Model parameters estimation and sensitivity by genetic algorithms. *Annals of Nuclear Energy*, 30(14):1437–1456.

Mohammad Zadeh, P., Sokhansefat, T., Kasaeian, A., Kowsary, F., and Akbarzadeh, A. (2015). Hybrid optimization algorithm for thermal analysis in a solar parabolic trough collector based on nanofluid. *Energy*, 82:857–864.

Myint-U, T. and Debnath, L. (2007). *Linear Partial Differential Equations for Scientists and Engineers*. Brikhauser Boston, Boston, 4th edition.

Nery, R. and Rolnik, V. (2007a). V. métodos híbridos para otimização global nãolinear. In *Congresso Nacional de Matemática Aplicada e Computacional Florianópolis, SC, Brasil*.

Nery, R. S. and Rolnik, V. (2007b). Métodos híbridos para otimização global não linear. In *Congresso Nacional de Matemática Aplicada e Computacional; Florianópolis, SC, Brasil*.

Park, E. and Zhan, H. (2001). Analytical solutions of contaminant transport from finite one-, two-, and three-dimensional sources in a finite-thickness aquifer. *Journal of Contaminant Hydrology*, 53(1):41–61.

Park, T.-Y. and Froment, G. F. (1998). A hybrid genetic algorithm for the estimation of parameters in detailed kinetic models. *Computers and Chemical Engineering*, 22:S103–S110. European Symposium on Computer Aided Process Engineering 8.

Poling, B., Prausnitz, J., and O'Connell, J. (2001). *The Properties of Gases and Liquids*. McGraw-Hill, New York, NY, 5th edition.

Sarkar, S., Roy, A., and Purkayastha, B. S. (2013). Article: Application of particle swarm optimization in data clustering: A survey. *International Journal of Computer Applications*, 65(25):38–46. Full text available.

Schwaab, M. and Chalbaud, E. (2008). Nonlinear parameter estimation through particle swarm optimization. *Chemical Engineering Science*, 63(6):1542–1552.

Siepmann, J. and Siepmann, F. (2012). Modeling of diffusion controlled drug delivery. *Journal of Controlled Release*, 161(2):351–362. Drug Delivery Research in Europe.

Taylor, G. (1954). The dispersion of matter in turbulent flow through a pipe. *Royal Society*, 223(23):446–468.

Thongmoon, M. and McKibbin, R. (2006). A comparison of some numerical methods for the advection-diffusion equation. *Res. Lett. Inf. Math. Sci.*, 10:49–62.

Thongmoon, M., McKibbin, R., and Tangmanee, S. (2012). Numerical solution of a 3-d advection-dispersion model for pollutant transport. *Thai Journal of Mathematics*, 5.

Van Genuchten, M. T. (1982). *Analytical solutions of the one-dimensional convective-dispersive solute transport equation*. Number 1661. US Department of Agriculture, Agricultural Research Service.

Vergnaud, J. (1993). *Controlled drug release of oral dosage forms*. CRC Press, New York, NY, 1st edition.

Welty, J., Wicks, C., Wilson, R., and Rorrer, G. (2007). *Fundamentals of Momentum, Heat, and Mass Transfer*. Wiley, New York, NY, 5th edition.

Witkovsky, V. (2021). FindRoots: Matlab central file exchange. `https://www.mathworks.com/matlabcentral/fileexchange/55206-findroots`. Accessed: 2021-06-20.

Young, N. P. and Balsara, N. P. (2021). *Flory–Huggins Equation*, pages 1–7. Springer Berlin Heidelberg, Berlin, Heidelberg.

Zadeh, P. M., Sokhansefat, T., Kasaeian, A., Kowsary, F., and Akbarzadeh, A. (2015). Hybrid optimization algorithm for thermal analysis in a solar parabolic trough collector based on nanofluid. *Energy*, 82:857–864.

Appendix A

Physical and chemical properties

Table A.1: Physical and chemical properties of α-pinine, eucalyptol and PLC (for Biotechnology Information, 2021b,a; Hansen, 2012; Welty *et al.*, 2007) .

Properties	α-pinene	eucalyptol	PLC
Vapor Pressure at 25 °C (mmHg)	4.75	1.9	-
Density at 25 °C ($\mathrm{kg \cdot m^{-3}}$)	859.2	926.7	1145
Molar volume ($\mathrm{cm^3 \cdot mol^{-1}}$)	159.5	167.5	-
δ_D ($\mathrm{MPa^{1/2}}$)	16.9	16.7	-
δ_P ($\mathrm{MPa^{1/2}}$)	1.8	4.6	-
δ_H ($\mathrm{MPa^{1/2}}$)	3.1	3.4	-
δ_T ($\mathrm{MPa^{1/2}}$)	17.3	17.7	20.2
Molar mass ($\mathrm{g \cdot mol^{-1}}$)	136.23	154.25	-

Table A.2: Physical and chemical properties of air (Çengel and Ghajar, 2015).

Properties	air
Molar mass ($\mathrm{g \cdot mol^{-1}}$)	29
ρ at 25 °C ($\mathrm{kg \cdot m^{-3}}$)	1.1948
μ at 25 °C ($\mathrm{Pa \cdot s}$)	1.83

Appendix B

Illustrative example

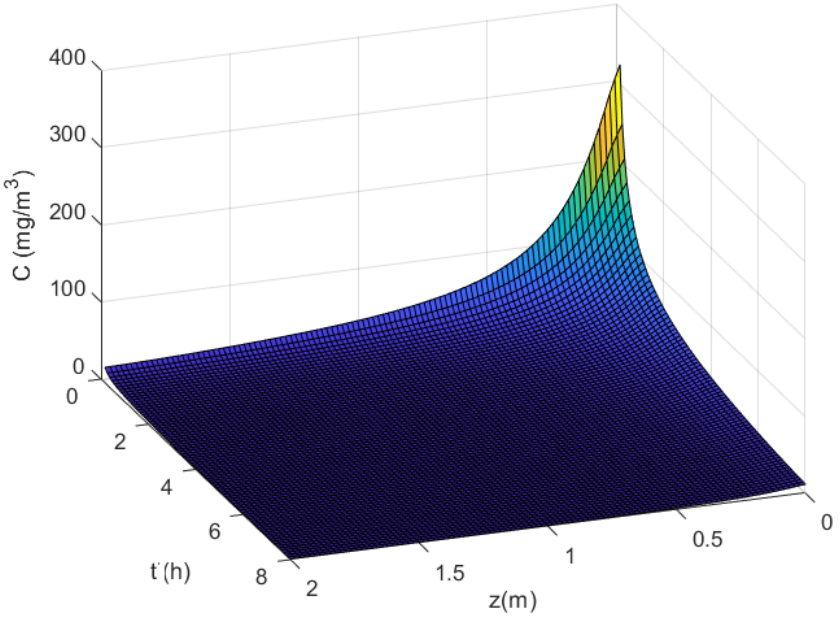

Figure B.1: 3 D representation of the concentration in the center of the tunnel, for various times between 10 min and 8h..

Appendix C

Active ingredient release

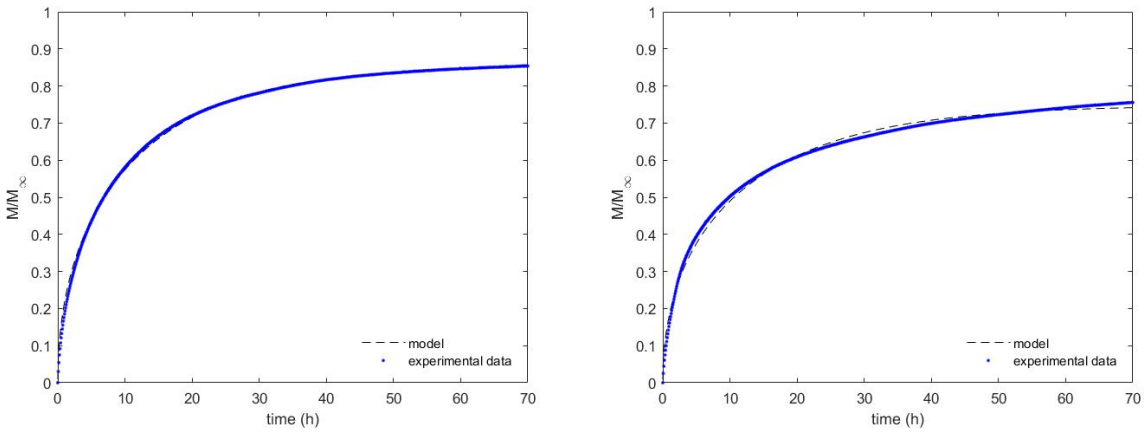

(a) Exp4-replica I

(b) Exp4-replica II

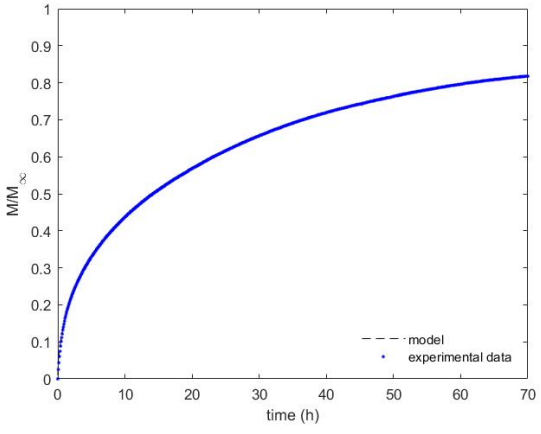

(c) Exp5-replica I

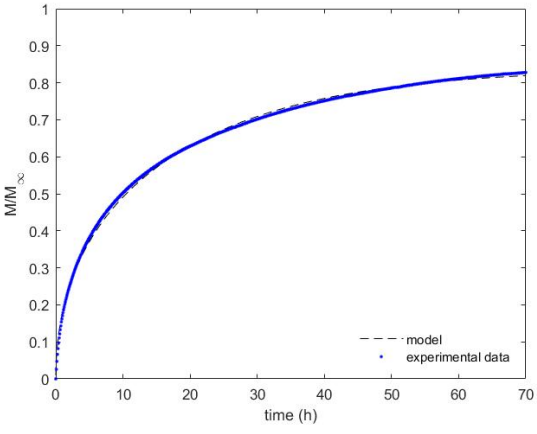

(d) Exp5-replica II

Figure C.1: α-pinene release experimental fitting.

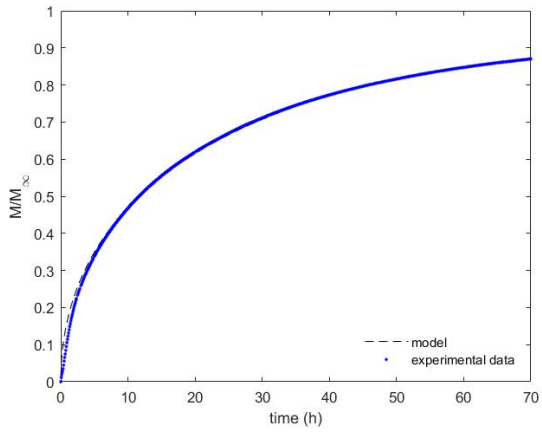

(a) Exp7-replica I

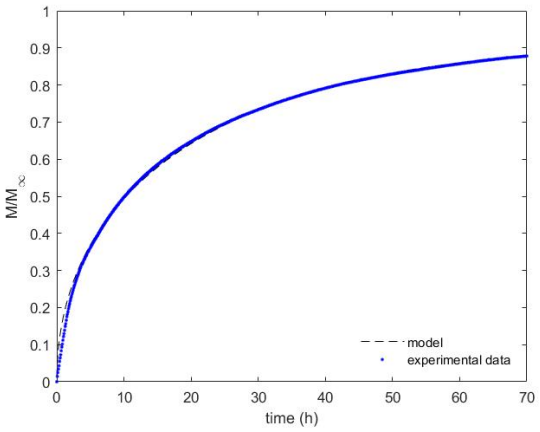

(b) Exp7-replica II

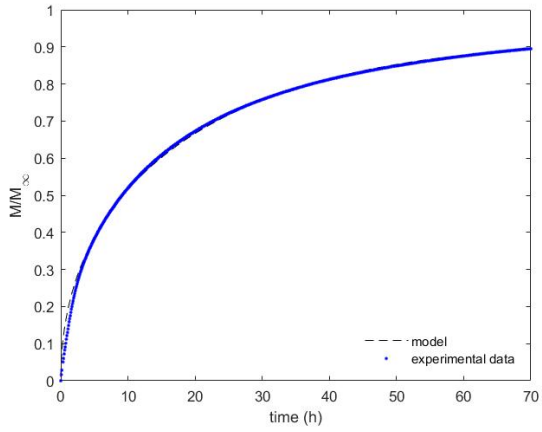

(c) Exp8-replica I

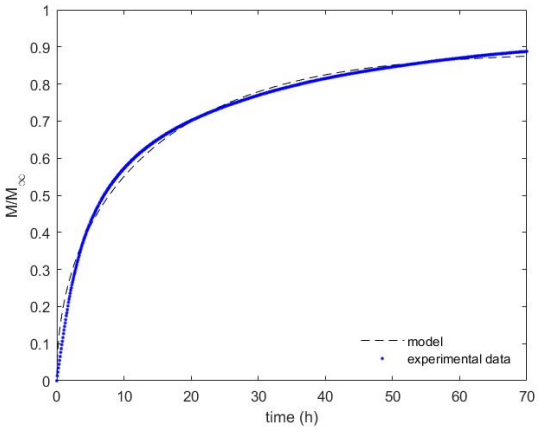

(d) Exp8-replica II

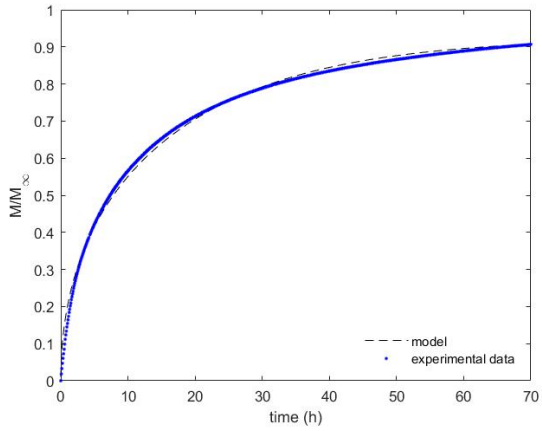

(e) Exp9-replica I

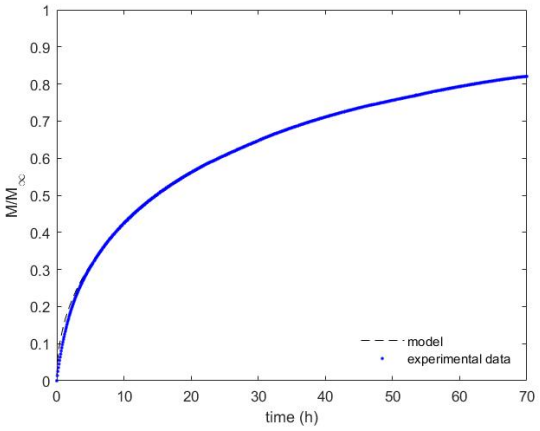

(f) Exp9-replica II

Figure C.2: Eucalyptol release experimental fitting.